11-2016

Functional MRI in the presence of repetitive, sub-concussive impacts

Trey E. Shenk
Purdue University

Graduate School Form
30 Updated 12/26/2015

PURDUE UNIVERSITY
GRADUATE SCHOOL
Thesis/Dissertation Acceptance

This is to certify that the thesis/dissertation prepared

By Trey E. Shenk

Entitled
FUNCTIONAL MRI IN THE PRESENCE OF REPETITIVE SUBCONCUSSIVE IMPACTS

For the degree of Doctor of Philosophy

Is approved by the final examining committee:

Thomas M. Talavage Chair	Joaquin Goni Cortes
Eric A. Nauman	Charles A. Bouman
Michael D. Zoltowski	

To the best of my knowledge and as understood by the student in the Thesis/Dissertation Agreement, Publication Delay, and Certification Disclaimer (Graduate School Form 32), this thesis/dissertation adheres to the provisions of Purdue University's "Policy of Integrity in Research" and the use of copyright material.

Approved by Major Professor(s): Thomas M. Talavage

Approved by: Venkataramanan Balakrishnan 12/05/2016

Head of the Departmental Graduate Program Date

FUNCTIONAL MRI IN THE PRESENCE OF REPETITIVE, SUB-CONCUSSIVE IMPACTS

A Dissertation

Submitted to the Faculty

of

Purdue University

by

Trey E. Shenk

In Partial Fulfillment of the

Requirements for the Degree

of

Doctor of Philosophy

December 2016

Purdue University

West Lafayette, Indiana

To my supportive parents, Mike and June Shenk, without whom this would not have been possible.

And to Emily Sleek for encouraging me through the process.

ACKNOWLEDGMENTS

I would like to especially thank my advisor, Thomas M. Talavage, for the long hours he spends mentoring his students. I would also like to thank Eric Nauman for his optimism and excitement and Greg Tamer for his constant help with scanning (and many interesting conversations). I would also like to thank Mimi Boutin, Jan Allebach, Okan Ersoy, and Xiaojun Lin for their guidance during my time as a TA. I would like to express my warmest gratitude to my labmates for their friendship and help with research: Kausar Abbas, Meghan Robinson, and Victoria Poole, as well as Sumra Bari, Bobby Chun, Allen Diaz, Pratik Kashyap, Ikbeom Jang, Xianglun Mao, Nicole Vike, and Diana Svaldi. Lastly, I would like to thank the people of Lighthouse Baptist Church for being a family to me in my time so far away from home.

TABLE OF CONTENTS

Page

Page

LIST OF FIGURES

ABSTRACT

Shenk, Trey E. PhD, Purdue University, December 2016. Functional MRI in the Presence of Repetitive, Sub-Concussive Impacts . Major Professor: Thomas M. Talavage.

Recent research has raised understanding and awareness of the long-term risks associated with mild traumatic brain injury (mTBI). While much research has focused on the role of concussion (a single event exhibiting clear clinical symptoms), the role of repetitive sub-concussive impacts is not well understood. This study uses functional MRI measurements of high school football players to identify functional changes, even in the absence of clinical symptoms.

1. INTRODUCTION

1.1 Mild traumatic brain injury in sports

1.1.1 Occurence of mTBI

It is estimated that 300,000 sports-related concussions occur annually [1]. Marar et al. estimated the rate of concussion for high school football players to be 22.9 per 10,000 exposures for competitions, 3.1 for practice, and overall 6.4 (with an athletic exposure defined as a game or practice). This is over twice the overall average rate among high school boys in sports of 3.1 per 10,000 athletic exposures (football included in average). Despite the frequent occurrence of concussion, diagnosing concussion has a certain level of uncertainty. The development of new technologies and methods have revealed that certain types of mTBI, were going undiagnosed [2]. For athletes who have received some external force to the head, symptoms such as loss of consciousness, post-traumatic amnesia, and periods of confusion provide the clearest indications of mTBI.

1.1.2 Potential risk despite absence of mTBI

Menon et al. went on to say that the presence of neuropsychiatric symptoms (e.g. depression, apathy, aggression), though known sequelae of TBI, were not sufficient for diagnosis of a concussion [2]. These clinical definitions put some contact-sports athletes in a unique position: they do experience regular physical insult, they may experience altered psychological or emotional states, but there may not be symptoms related to a singular event. Therefore, in the absence of obvious symptoms, the athletes are not diagnosed with a concussion and could be considered healthy. However, McKee et al. found cases of chronic traumatic encephalopathy (CTE) in

athletes without a history of concussions [3]. This would suggest that subconcussive events experienced by these athletes may be sufficient to cause a neurodegenerative cascade [4].

1.1.3 Advanced imaging techniques

In the absence of clear symptoms or events, advanced imaging techniques can provide insight concerning subtle neurologic changes. The Purdue Neurotrauma Group has already found changes in contact sport athletes using MRS, functional MRI (fMRI), and resting state fMRI (rs-fMRI) [5–12]. More work is needed to refine the existing techniques and apply new methods to the existing imaging data.

1.2 Current Work

The current work has utilized advanced imaging techniques to detect injury using a hemodynamic reponse (HDR) task, a visual spatial memory task, and a resting state scan. Changes in the ability of the vasculatur to respond to neural activity and characteristics of that response would be observed in the HDR task. Changes in location of spatial memory encoding and in response levels necessary to perform the task would be exhibited in the visual memory task. The resting state was chosen as an exploratory method, with analysis involving comparison of canonical networks across sessions and the magnitude of internetwork correlation. This work shows that changes can be found in contact sport athletes who do not show clinical symptoms, suggesting that repetitive subconcussive head acceleration events can result in pre-symptomatic injury in athletes.

2. BACKGROUND

2.1 Mild traumatic brain injury

2.1.1 Current definition of mild traumatic brain injury and concussion

There are an estimated 1.7 million cases of traumatic brain injury (TBI) annually, with an estimated cost of $60 billion in 2000 [13,14]. Concussion and mild TBI (mTBI) are often used interchangeably in the US literature and are lowest on the spectrum of TBI. The definition of concussion given by the 4th International Conference on Concussion in Sport is [15]:

> Concussion is a brain injury and is defined as a complex pathophysiological process affecting the brain, induced by biomechanical forces. Several common features that incorporate clinical, pathologic and biomechanical injury constructs that may be utilised in defining the nature of a concussive head injury include:
>
> 1. Concussion may be caused either by a direct blow to the head, face, neck or elsewhere on the body with an 'impulsive force transmitted to the head.
> 2. Concussion typically results in the rapid onset of short-lived impairment of neurological function that resolves spontaneously. However, in some cases, symptoms and signs may evolve over a number of minutes to hours.
> 3. Concussion may result in neuropathological changes, but the acute clinical symptoms largely reflect a functional disturbance rather than a structural injury and, as such, no abnormality is seen on standard structural neuroimaging studies.

4. Concussion results in a graded set of clinical symptoms that may or may not involve loss of consciousness. Resolution of the clinical and cognitive symptoms typically follows a sequential course. However, it is important to note that in some cases symptoms may be prolonged.

McCrory et al. also notes that most symptoms of concussion resolve within 7-10 days [15]. If symptoms do not resolve within three weeks, the injury can be considered an mTBI [16].

2.1.2 Disturbances caused by mTBI

The occurrence of mTBI is characterized by a series of ionic, metabolic, and structural alterations resulting from significant mechanical insult. Shear and strain forces cause a disruption in the brain's ionic homeostasis, resulting in an increase in intracellular calcium and extracellular potassium as shown in Figure 2.1 [17]. This is accompanied by hypermetabolism as pumps work to restore ionic balance. This short period of hypermetabolism is followed by a lingering state of hypometabolism, characterized by a reduced rate of glycolysis and diminished cerebral blood flow.

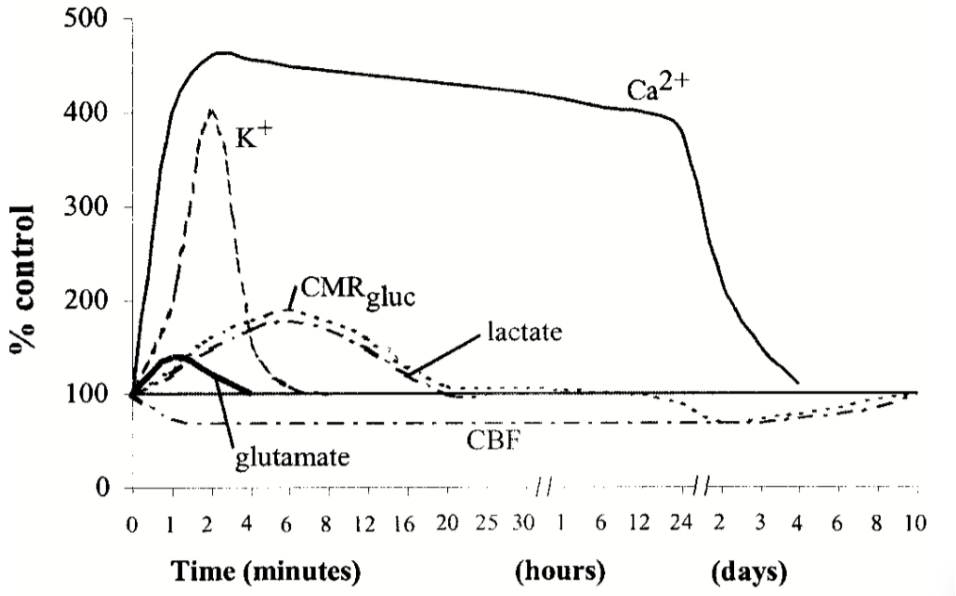

Fig. 2.1. Neurometabolic cascade reported by [18].

In addition to neurometabolic changes, diffuse axonal injury can also be present. While once thought to be the dominant form of injury in mTBI, the current literature suggests a weak connection of axonal injury and concussive symptoms [19]. Ommaya et al. estimated that a threshold for angular acceleration of 12,500 rad/s^2 is necessary to cause diffuse axonal injury, while accelerations of 4500 to 5500 rad/s^2 are sufficient to cause a concussion [20, 21].

2.1.3 Period of vulnerability

Animal studies using rats involving single and multiple concussions have suggested that a biphasic model is appropriate for mTBI, as illustrated in Figure 2.2 [22]. It is suggested that the lingering hypoactive state may present a time of vulnerability, when the brain is less able to compensate for further injury. This finding is also reported by Yoshino et al., who observed a metabolic depression for up to ten days [23]. The cause of this depression is not known, though it could be a result of dysregulation

caused by the injury, calcium or lactate accumulation that is also present post-injury, or disruption of cerebral blood flow.

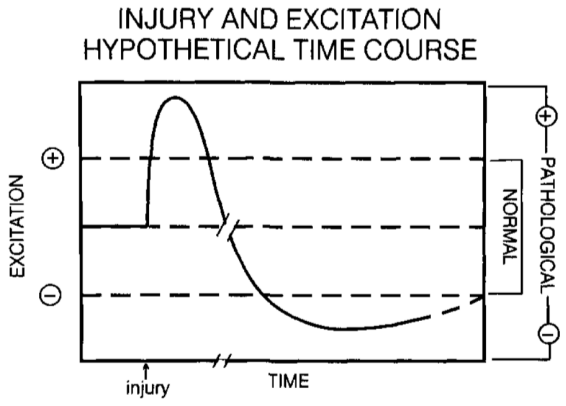

Fig. 2.2. Levin et al. hypothesized this altered level of excitation in response to mechanical injury [22].

Longhi et al., in another rat study, found that receiving a second concussion three to five days after the initial injury exhibited significantly decreased performance, along with more pronounced axonal disruption [24]. However, even rats with only a single injury exhibited observable histopathological abnormalities. When the second concussion occurred five days after the first injury, performance and axonal disruption matched that of rats with only a single injury, suggesting that there is a window of vulnerability following mTBI. In a similar finding, Laurer et al. reported a twenty-four hour period of increased vulnerability following an initial injury [25]. Neither Longhi et al. or Laurer et al. indicate an estimated time period for the resolution of this vulnerable phase. It is not apparent how, or even if, the timing observed in rats studies would translate to humans.

2.1.4 Concussion in young athletes

Clinicians and physical trainers are continuing to learn how to best prevent and treat mTBI in youth sports. The time required for return-to-play following an injury

is critical to the health of the athletes. One study found that 53% of high school football athletes returned to play in 7-9 days post-injury, with 26% returning in 3-6 days [1]. The appropriate amount of time is case-dependent. Field et al., when comparing results from neurocognitive tests, found that college athletes returned to control levels after three days, while high school athletes took seven days to return [26]. This could mean that high school athletes are vulnerable even longer than college or adult athletes.

2.1.5 The risk of repetitive head injury

Putting these together, it is clear that mTBI causes significant changes that make the brain prone to further, immediate injury. Furthermore, young athletes seem to be more at risk compared to college athletes in the short term. The long-term effect of mTBI is not known, but it is theorized that injuries increase the rate of age-related cognitive decline, as shown in Figure 2.3. In a study of former athletes (ages 40-70) from Division III schools, history of concussion was was found to be inversely related to executive function and directly related to anxiety, depression, alcohol use, sleep disturbance, emotional dyscontrol, and fatigue [27].

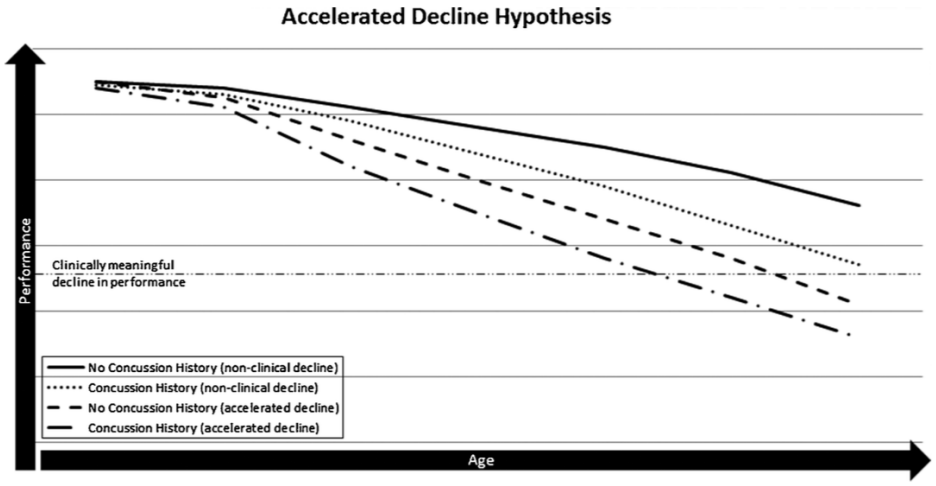

Fig. 2.3. The accelerated decline theory put forth by [28] stating that the normal decline of aging can be hastened following TBI. Concussion history is expected to be a contributor to this decline, though large deviations in the trend are expected.

The role of subconcussive injury also needs further exploration. Athletes can be "dinged" during play, but unless they show clear symptoms (loss of consciousness, amnesia, nausea, etc.), they will most likely not be diagnosed as concussed. However, this idea of a binary injury classification is almost certainly flawed, as most injuries follow a continuum. There is certainly a threshold of TBI above which readily observable symptoms are present, but this does not mean that a lack of these symptoms indicates that the player is completely healthy.

It is reasonable to propose that the period of vulnerability following a mTBI may also be present after athletes experience heavy mechanical insult, even in the absence of clinical symptoms. Given the prolonged period of recovery necessary for young athletes, it is imperative that further research be conducted to better understand the brain's stages of injury and recovery.

2.1.6 Head impact telemetry

Advancements are being made in the field of head impact telemetry. Products available now include HITS (Riddell), Brain Sentry (now know as Common), Hammerhead Mouth Guard (i1 Biometrics), Safe Brain, Shockbox (Impakt Protective), Checklight (Reebok), and GForceTracker. If the changes observed in imaging studies are due to the contact received during play, it should be possible to model the deviations as a response to hits received during play. However, modeling the relationship between head acceleration events and advanced imaging measurements has proven to be challenging. The data (both imaging and hits) are noisy, studies generally have a small sample size, and the relationship is most likely non-linear, making the modeling process difficult. But as additional data are gathered, trends and relationships should become clearer.

2.1.7 Towards the goal of making contact sports safer

To properly inform trainers and coaches of the risks faced by athletes, a clear relationship must be established between readily observable events and neuronal function. It is not feasible to expect every athlete to receive regular medical imaging due to the staffing and monetary commitment necessary to collect and analyze the data. However, it would be reasonable to put sensors in helmets to collect collision events during play. Therefore, once a relationship between these observable collisions and functional changes is found, coaches can choose practice and in-play strategies that will protect the long-term health of the athletes.

2.2 Basics of BOLD fMRI

2.2.1 The BOLD signal

The MR signal can be expressed as functions, f_1 and f_2, of the longitudnal and transverse relaxation [29]:

$$S = \sum_i S_{0_i} f_1(T^*_{1i}) f_2(T^*_{2i}) \tag{2.1}$$

Where S_{0_i} is the spin density in the i^{th} compartment, T^*_{1i} and T^*_{2i} are the apparent longitudinal and transverse relaxation constants. The transverse relaxation constant, T^*_{2i}, is affected by changes in the paramagnetic contents of the compartment, which will alter the local field homogeneity. Specifically, BOLD fMRI exploits the concentration of deoxygenated hemoglobin, which is related to neural activity and has a direct effect on the local T^*_{2i}. The MR signal in relation to the transverse relaxation can be written as

$$S = S_0 e^{\mathrm{TE}/\mathrm{T}^*_2} \tag{2.2}$$

Where S_0 is the signal in the absence of transverse relaxation [30]. The fractional signal change from baseline to activation can be written as

$$\frac{\Delta S}{S_{\text{baseline}}} = \frac{S_{\text{activation}} - S_{\text{baseline}}}{S_{\text{baseline}}} \tag{2.3}$$

$$= \frac{S_0 e^{\mathrm{TE}/\mathrm{T}^{*\prime}_2} - S_0 e^{\mathrm{TE}/\mathrm{T}^*_2}}{S_0 e^{\mathrm{TE}/\mathrm{T}^*_2}} \tag{2.4}$$

$$= e^{\mathrm{TE}/\mathrm{T}^{*\prime}_2 - \mathrm{TE}/\mathrm{T}^*_2} - 1 \tag{2.5}$$

$$= e^{(\mathrm{TE})(\Delta \mathrm{R}^*_2)} - 1 \tag{2.6}$$

Where $\mathrm{T}^{*\prime}_2$ is the transverse relaxation time during activation, and $\Delta \mathrm{R}^*_2$ is the difference in transverse relaxation rates, $1/\mathrm{T}^{*\prime}_2 - 1/\mathrm{T}^*_2$. For small values of $(\mathrm{TE})(\Delta \mathrm{R}^*_2)$, the last line can be approximated by

$$\frac{\Delta S}{S_{\text{baseline}}} \approx (\mathrm{TE})(\Delta \mathrm{R}^*_2) \tag{2.7}$$

We can see that for small values, the fractional change in signal strength will change linearly with the change in transverse relaxation rates. It is also known that

the transverse relaxation rate will change based on the local concentration of deoxygenated hemoglobin due to changes in field inhomogeneities. As was demonstrated by Ogawa et al., $T_2^\star$-weighted images can exploit the field distortions caused by deoxygenated hemoglobin to generate images that depend on the local blood oxygen content [31].

2.2.2 Task-based fMRI analysis

LTI analysis of the BOLD signal

How neural metabolism translates to changes the BOLD signal is not well understood. Early work by Kwong et al. illustrated the hemodynamic response to a stimulus, as shown in Figure 2.4.

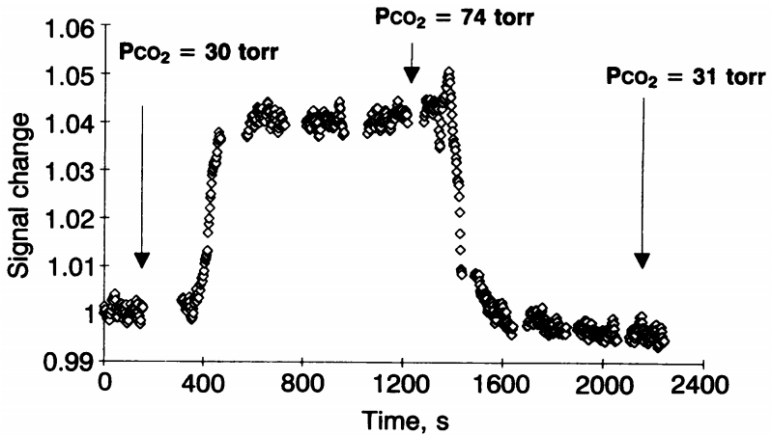

Fig. 2.4. BOLD response in a rabbit brain to a change in the partial pressure of CO_2.

The response is characterized by a delayed increase in signal, followed by an undershoot, with some studies also observing a small intial dip (not observable in Figure 2.4). The balloon model by Buxton et al. modeled deoxygenated hemoglobin content, intra- and extra-vascular cerebral blood volume effects, and a slow recovery rate of venous cerebral blood volume post-stimulus (see Figure 2.5) [32].

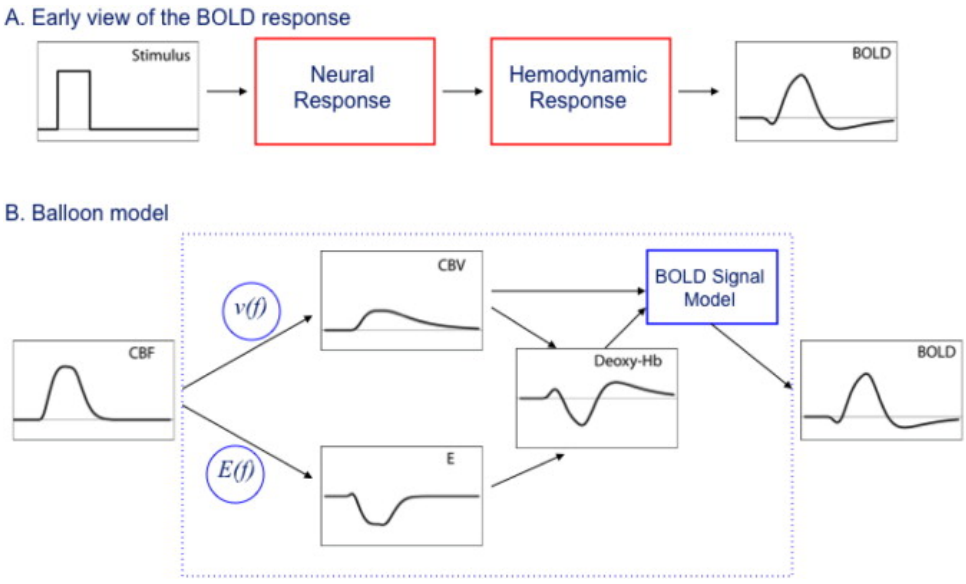

Fig. 2.5. Note that $v = f^{\alpha}$, where v and f are CBV and CBF normalized to their baseline values, and $\alpha = 0.68$ (value estimated from the data) [33].

While work continues to find a mechanistic model relating neural activity to BOLD signal, current fMRI analysis techniques use a black box approach, using a simple relationship between stimulus and BOLD to localize and quantify activation. Dale et al. demonstrated that the output BOLD is roughly linear to the stimulus, even with two second inter-trial spacing [34]. This characteristic makes it possible to model the signal as the output of a linear time-invariant system with an appropriately chosen impulse response:

$$y(t) = h(t) * s(t) + e(t) \tag{2.8}$$

Where $y(t)$ is the observed signal, $s(t)$ is loosely defined as neural activity, $h(t)$ is the impulse response (known as the hemodynamic response function, or HRF), and $e(t)$ is the observed error. AFNI (Analysis of Functional Neuroimages, a software package developed at the National Institute of Health) uses the HRF defined as (Figure 2.6)

$$h(t) \propto t^{q} e^{-t} \tag{2.9}$$

where q is chosen to be 4.

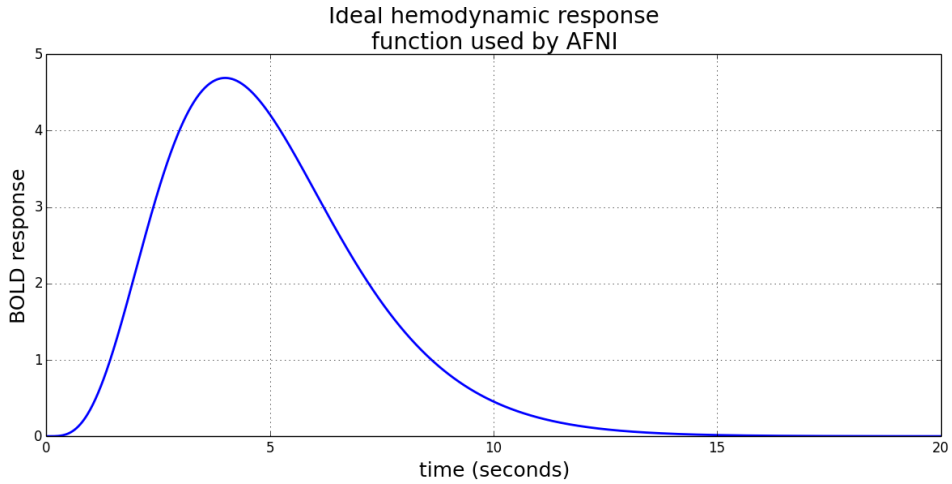

Fig. 2.6. Ideal HRF from AFNI. The y-axis is in arbitrary units and will be scaled to a convenient value processing.

The HRF will be scaled so that resulting statistics will be in units (again arbitrary) of percent signal change. The input, $s(t)$, is generally an indicator function, equaling one during the performance of a task and zero otherwise. This simplistic model has been used to accurately estimate and localize neural activation in task fMRI. Early work, like that by Bandettini et al., demonstrated this type of relationship between task performance and BOLD signal, as shown in 2.7 [35]. Furthermore, the signal was shown to be roughly linear in response to stimulus presentation [36].

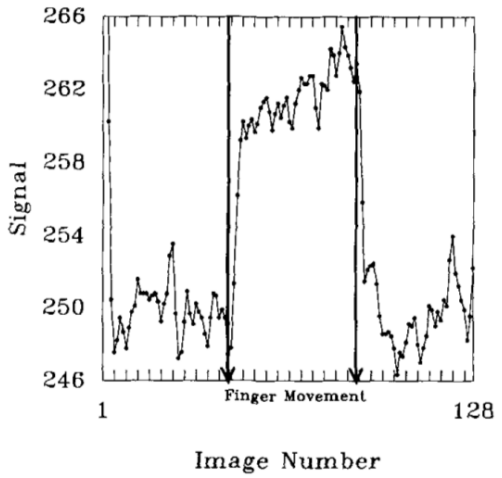

Fig. 2.7. Early BOLD fMRI signal by [35] .

Statistical analysis of task fMRI

The next step is to define a model which lends itself to statistical analysis. The fMRI field relies almost entirely on the general linear model (GLM) when performing statistics [37]. A single voxel time series is modeled as

$$\mathbf{y} = \mathbf{X}\boldsymbol{\beta} + \boldsymbol{\epsilon} \tag{2.10}$$

where $\mathbf{y}$ is the voxel time series, $\mathbf{X}$ is the design matrix with each column representing a stimulus or noise regressor, $\boldsymbol{\epsilon}$ is the error, and $\boldsymbol{\beta}$ is the regressor weighting vector to be estimated. Using the estimated $\hat{\boldsymbol{\beta}}$, a hypothesis test can be performed that will compare a task to a given baseline. For example, a t-test can be performed, where the t-statistic is given by

$$t = \frac{\mathbf{c}^T\boldsymbol{\beta}}{\sqrt{var\left(\mathbf{c}^T\boldsymbol{\beta}\right)}} \tag{2.11}$$

with $\mathbf{c}$ as a contrast vector.

The contrast vector can be chosen to test the significance of only one task regressor by having a single one with the rest of the entries zero, a difference of activation by having both a positive and negative one, or any linear combination is desired. More

details will be given in "N-back as a prototypical example" of how to choose this vector.

Because this analysis is done across all voxels independently, it is called a massive univariate analysis. In the fMRI field, univariate analysis refers to voxel-by-voxel testing, while multivariate would mean that multiple voxels are being testing at once (most univariate models will have multiple explanatory regressors in the design matrix). Usually, univariate analysis is performed initially, forming statistical parameter maps (SPM, not to be confused with the software package). These SPMs can be individual β coefficients and t-scores for the specific regressors, full model F-statistics, or results of general linear tests (whether t-tests or F-tests).

Multiple comparisons correction

Because of the exceptionally large number of tests performed, multiple comparisons correction is necessary. Some standard approaches for voxelwise correction would be Bonferroni or false discovery rate (FDR). However, the incorrect assumption of independent tests makes these corrections too conservative, with only large effects being able to survive.

Another approach is to correct on a cluster level. A cluster is a contiguous group of voxels following an applied threshold. AFNI uses a cluster simulation method that generates datasets under the null hypothesis to build a distribution of a statistic. Given a specific threshold (one threshold for the entire map), it can give α values for a cluster of a specific size. This process is described in more detail in Appendix A.2.

A different software package, developed at the Oxford Centre for Functional MRI of the Brain (FMRIB), FSL (FMRIB Software Library) can perform these types of randomization tests, but FSL also has a "threshold free cluster enhancement" method [38]. This method operates on the principle that a small effect size with large coverage can be just as significant as a large effect size with a small area. It

is essentially taking a type of cluster mass into consideration, rather than a simple threshold.

None of these tools will perfectly control the error rate, and they all make assumptions. It is up to the researcher to be versed in the particular assumptions and pitfalls associated with the specific method being used.

N-back as a prototypical example

The steps of processing task-based fMRI will be described using an example N-back task. In N-back is a common working memory task used in fMRI The positive condition is when the current stimulus matches the stimulus N before. This example will use N-back tasks, where ($N \in \{0, 1, 2\}$).

Each voxel of the scan data is modeled using a general linear model.

$$\mathbf{y} = \boldsymbol{X}\boldsymbol{\beta} + \mathbf{e} \tag{2.12}$$

Where $\boldsymbol{y}$ is the voxel time series, $\boldsymbol{X}$ is the design matrix, $\boldsymbol{\beta}$ is the vector of regressor weights to be estimated, and $\boldsymbol{e}$ is the additive noise. An example voxel time series is shown in Figure 2.8 and an example design matrix is shown in .

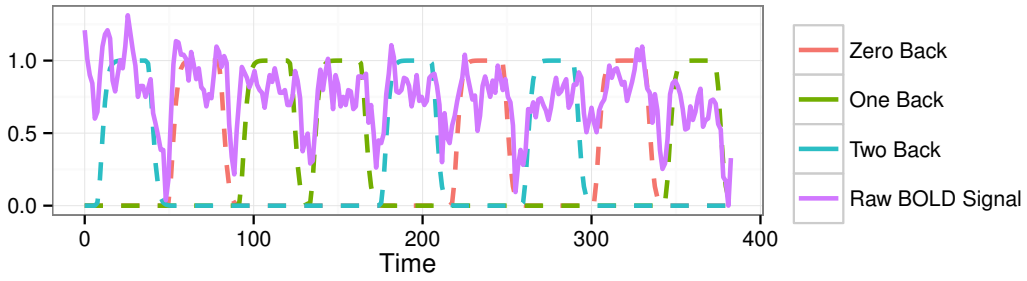

Fig. 2.8. Raw BOLD signal compared to the presented tasks. There is a clear relationship between the task and measured signal.

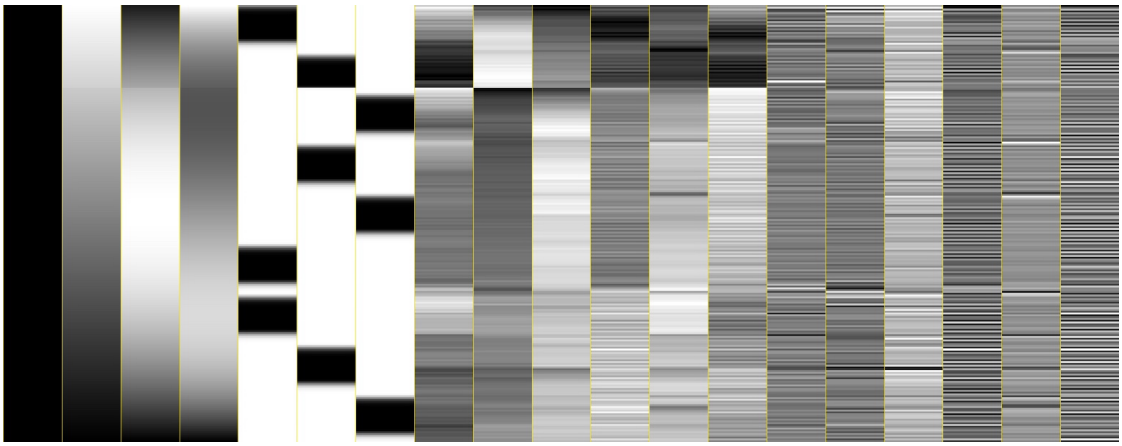

Fig. 2.9. Example design matrix, with darker colors being more positive. The motion regressors on the right are unique to each scan.

The design matrix has three components: the first four columns are polynomials to describe drift, the next three columns are the task regressors, and the last twelve are motion regressors (six to handle translation and rotation, and their six temporal derivatives).

Tests can be performed on the resulting β coefficients as described in Section 2.2.2. Differences in activation can be tested for by using the contrast vector. If the columns of X refer to the zero-back, one-back, and two-back tasks, the contrast vector $\mathbf{c} = [-1, 0, 1]$ could test whether the 2-back was significantly different than the zero-back, referred to as the two-vs.-zero back contrast. These types of tests can be easily coded into the analysis using AFNI's afni_proc.py function (the actual test will be performed using 3dDeconvolve).

The output of this analysis will be a bucket dataset that contains an F-score, and β values with their associated t-statistics. The t-statistic should be viewed as a measure of the confidence in the measurement. If thresholding is to be performed, it is advisable to perform it on the t-statistic. The β coefficients show the effect size related to the regressor. If scaling is done properly in the analysis, the β should be in arbitrary units of percent signal change. These are considered consistent if the

experiments are performed with the same protocol, scanner, and coil. They can then be used to compare across subjects, however, it is not considered "good practice" to compare the values of percent signal change across scanners and configurations.

When displaying and interpreting these values, it is best to threshold on the t-statistic and set the display color using the β. While it is important to know where there is a high degree of confidence, it is also vital to know the effect size. It could be that the effect size is small enough to be ignored, though it is significant, or the effect size could be unreasonably large, indicating problems with the preprocessing.

2.2.3 Resting state fMRI and independent component analysis

Resting state

Though task-based fMRI is a logical method of mapping the brain's functional topology, it does not tell the whole story. During rest, the brain accounts for 20% of the body's expended energy, and during a task that increases by <5% [39]. Furthermore, effects from task-based scans can be altered based on subject task participation, task proficiency, arousal level, and cognitive health. If an injured population is to be studied, it may not be possible for the subjects to complete a demanding task.

Resting state presents a way to study populations without the complication of task compliance. During rest, spontaneous neuronal activity is thought to be related to the intrinsic connectivity between neural populations. Two popular methods to investigate this connectivity are seed-based analysis and independent component analysis (ICA). Seed-based methods have proven to be robust and provide consistent measures across groups. However, they depend on the choice of the seed region and only look at a single network. ICA performs blind source separation (BSS) to find multiple networks without the assumption of seed regions. Smith et al. showed that these connectivity networks have a strong association to different behavioral domains, including variations of action, cognition, emotion, and perception [40].

Probabilistic Independent Component Analysis

The basic setup for ICA is the generative model

$$\mathbf{x} = \mathbf{As} \tag{2.13}$$

where $x_j = a_{j,1}s_1 + a_{j,2}s_2 + \ldots + a_{j,n}s_n$, $a_{i,j}$ being the latent mixing variables and s_i being the individual component. This model can be inverted to form

$$\mathbf{s} = \mathbf{Wx} \tag{2.14}$$

where $\mathbf{W}$ is the unmixing matrix.

The components are estimated by finding a linear combination of x_j that maximizes resulting non-Gaussianity of the source signals and their spatial independence [41].

Early implementations of ICA used the model $\mathbf{X} = \mathbf{AS}$, where X is a $p \times n$ matrix of n measured signals, each containing p time points. This model is similar to the GLM, but the square mixing matrix $\mathbf{A}$ must be estimated. In practice, the lack of a noise source in the model made the output sensitive to small perturbations in the input [42]. For example, ICA analysis of tasks with known activation patterns may show the active regions fragmented across networks.

The model for probabilistic ICA (PICA) is

$$\mathbf{x}_i = \mathbf{As}_i + \boldsymbol{\mu} + \boldsymbol{\eta}_i \tag{2.15}$$

where $\mathbf{x}_i$ is a vector of p observations from the ith voxel, $\boldsymbol{\eta}$ is additive Gaussian noise. The noise covariance is estimated for each voxel, allowing the model to account for the differing levels of noise that is present across tissue types.

An example of the networks found using a twenty component PICA is shown in Figure 2.10. Of the twenty components estimated for Figure 2.10, ten were considered to be "well matched," and the other components were considered to be fragments or noise. These well-matched networks represent the canonical resting state networks (RSNs) and have been reproduced in multiple ICA studies [43–45].

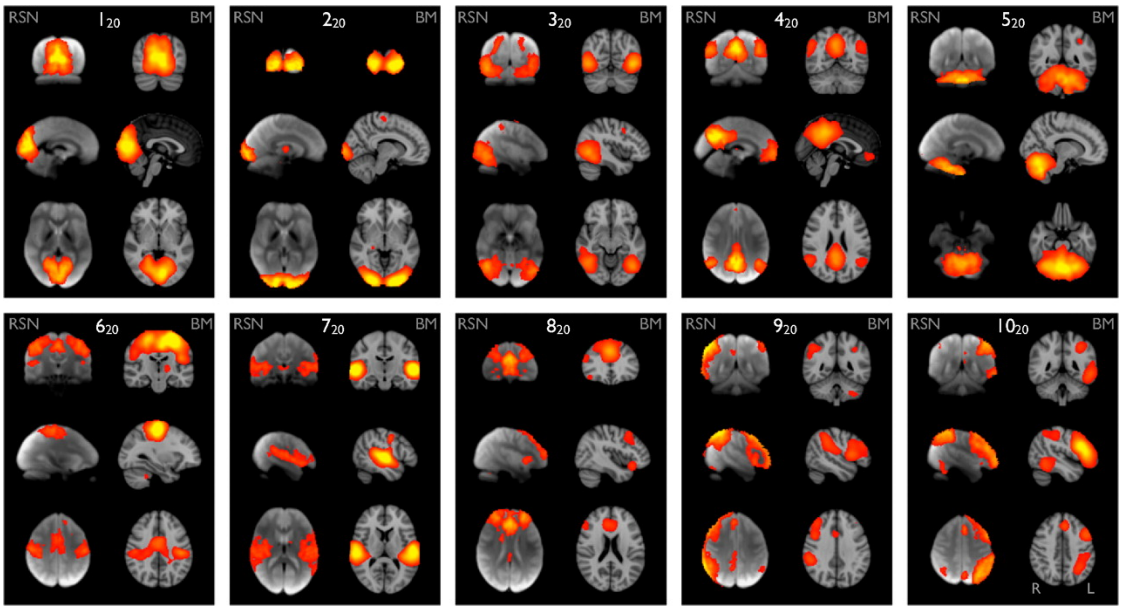

Fig. 2.10. Ten consistent networks found by [40].

2.3 Challenges facing fMRI

The field of fMRI is going through growing pains as methods continue to mature and standard practices are being set. Part of the difficulty is the wide range of skills needed to improve methods. Physicists and engineers with an in-depth understanding of MR physics are needed to improve equipment, giving better quality scans (increased SNR and CNR, reduced TR, fine voxel size, ...). Mathematicians and statisticians are needed to develop new methods to deal with the unique problems that are present in this data analysis. Psychologists can give insight into the proper design and analysis of experiments, including high-quality testing paradigms and task organization. And medical doctors and researchers are necessary to tie the results of the experiments to the physiology, as well as bridging the gap between research and medical practice.

2.3.1 The good and bad at the bleeding edge

The op-ed letter "This is Your Brain on Politics" is an example of results that are damaging to the field, though made with the (most likely) best intentions of the researchers involved [46]. It made big claims with the support of fMRI, including linking feelings of peril or disgust to the Republican party and stating that the voters felt conflicted about Hillary Clinton. These claims were accompanied with nicely rendered activations plots, as in Figure 2.11.

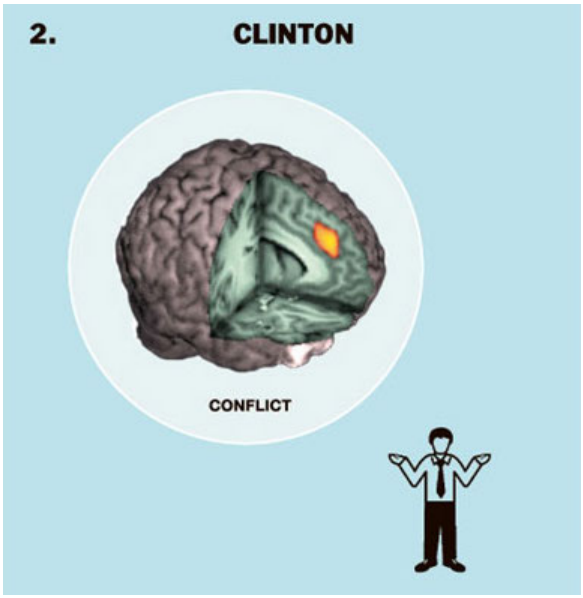

Fig. 2.11. Researchers claim to have localized a specific "conflict" region.

While a generally popular op-ed, neuroscientists were quick to point out the large flaws in the study. A group of seventeen neuroscientists published an op-ed in response just three days later [47]. They called the claims "scientifically unfounded" and stated their misgivings that it was published without any kind of peer-review. While it is important to educate the public about the direction that scientific research is taking, care must be taken to not give these kinds of false claims that will ultimately damage the scientific community's relationship to the public.

On the other extreme, the journal paper "Using fMRI to decode true thoughts independent of intention to conceal" by Yang et al. gives an example of a more rigorous study [48]. A multivariate pattern analysis procedure (based on a Gaussian Naive Bayesian classifier) was trained to distinguish between yes and no responses. After training the classifier, subjects were told to attempt to conceal their true response. The classifier still achieved median accuracies of 66%, 75%, and 78.5%. This is an impressive result (and one that warrants careful ethical discussions, such as the possible use of fMRI as an interrogation tool). Though perhaps not as flashy as "This is Your Brain on Politics," it is a good example of research that can move the community forward.

These two examples are good illustrations of what can happen at the boundaries of a research field. While early experiments focused on relatively straightforward hypotheses, such as areas of localized activation, now researchers are beginning to find correlates of specific thoughts (answer to yes/no questions) and brain activity. However, it can be damaging to the field when researchers reach too far without any prior justification. Media attention on poorly designed studies can miseducate the public, as well as create mistrust when claims are refuted. Though research is by definition new knowledge, researchers should be cautious when investigating claims that are far beyond the current level. Also, care should be taken when drawing conclusions to not overestimate the impact of the work in progress.

2.3.2 Continually developing statistical analysis

Modeling in fMRI is generally done at the voxel level, resulting in a massively univariate approach (many separate GLMs), yielding a large number of tests. The number of voxels in native space can easily exceed 100,000. This number can increase dramatically after performing resampling to form isotropic voxels. Given the large number of tests performed during analysis, correction for multiple comparisons must be performed. Some corrections, like Bonferroni and false-discovery-rate (FDR), are

too conservative and results will almost never show significant activations. More sophisticated methods involve random field theory, along with estimates of the spatial smoothness of the data, as well as brute-force simulation tests. However, it took time for the community to make widespread use of these methods.

At the 2009 meeting of the Organization for Human Brain Mapping (OHBM), one of the most consequential posters had been initially rejected as a prank. Bennett et al. presented results from a dead salmon that had been scanned while being presented with a series of pictures [49]. Following standard preprocessing, a cluster of three voxels were active, shown in Figure 2.12. The purpose of this poster was to emphasize the need for multiple comparisons correction to the fMRI community. Bennett et al. noted that there were no active voxels even at the ($p_{corrected} < 0.25$) level.

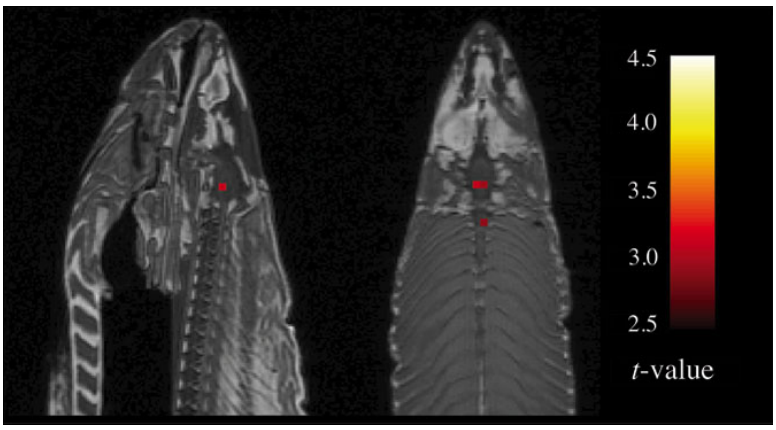

Fig. 2.12. Cluster of three active, in-brain voxels, thresholded at an uncorrected $p<0.001$.

Researchers in the community responded by reporting corrected p-values, as well as sharply criticizing those who did not use multiple comparison correction. The three major software packages (AFNI, SPM, and FSL) all include software to perform this correction. Seven years after Bennett et al., Eklund et al. called into question the current means of correction, claiming that the false positive rate, nominally 5%, could

be as high as 70% [50]. Regrettably, they overstated the impact of their findings, claiming that their findings brought doubt to the validity of the 40,000 studies to date. This was deeply troubling to researchers and was sensational enough to receive widespread media attention. The language of the article was soon changed to focus attention on those particular studies which were weakly significant, instead of the entire corpus of fMRI literature. It did bring to attention several incorrect assumptions held by the community, such as the current model of the autocorrelation (which in reality had a thicker tail than current models used) and the simplification that spatial smoothness was uniform (known to be false, but non-uniform spatial smoothness is difficult to estimate and incorporate). Cox et al. have responded to Eklund et al. by using more accurate models of the underlying autocorrelation function, including non-parametric methods to estimate p-values (a brute force method that uses null datasets generate from the model residuals), and developing ways to account for spatial non-uniformity [51].

2.3.3 Moving forward as a researcher

The challenge of small datasets (which is nearly unavoidable given the effort and expense required to collect the data), massive number of tests, and non-uniform structure of the data (particularly anisotropic, spatially-varying smoothness) has been daunting to the fMRI community. While the tools continue to grow in sophistication and accuracy, the validity of the research is ultimately the responsibility of the researcher. Investigators must be informed not only by statistical p-values, but by knowledge of physiology, biomechanical conditions, and common-sense when discussing the impliciations of their work. While it is easy to pass the blame to software packages, which can sometimes inflate p-values, the onus remains with the investigators to provide the scientific community with high-quality research. In the same way, the entire field cannot be disregarded due to a subset of the community producing substandard, though statistically significant, research.

3. INDIVIDUAL FLAGGING BASED ON VISUAL N-BACK TASK

Portions of this work were published in *Developmental Neuropsychology* [11]. Additional points are made here with clarification of some methods and with mention of future directions that this method could take.

3.1 Method goals

The goal of this project is to develop a flagging algorithm that will give some measure of a subject's level of deviation from a predefined norm. This would be a step in the direction of an individual measure indicating if a subject is possibly at risk. The results of this flagging can easily be combined with other measures, such as ImPACT, to provide a more accurate assessment of an athlete compared to a single test.

Several important assumptions were made during this project. They are:

1) *The beta contrast values in the pre-season were assumed to be identically distributed.*

   This would mean that the contrast values are consistent across subjects and that the subjects are in a healthy or stable state before the onset of contact practice. Studies have shown that the beta values are consistent across healthy subjects [52]. However, it is not clear whether these players can be considered healthy.

2) *Changes in the season of play that are outside of the confidence interval are abnormal.*

Again, the beta values do appear to be consistent across subjects, but the healthy range for these values is not clear.

3.2 Methods

3.2.1 Task presentation

The subject performed an N-back (N=0, 1, 2) task on a series of non-representational line-segment designs, presented via fiber optic goggles (NordicNeuroLab; Bergen, Norway). Nine task blocks (30s duration) were presented in a pseudorandom order, each comprising 15 image presentations (1500ms duration) at a rate of 0.5 Hz. Blocks were preceded by 12s of instructions indicating the category (i.e., N) of the task. Line drawings, which could not be readily verbalized, were used to discourage strategies that did not involve visual working memory [53].

3.2.2 Processing

AFNI was used to preprocess the data, including slice-timing correction, volume registration, and spatial smoothing (isotropic Gaussian, FWHM=4mm). After estimating the percent signal change due to each task, contrast maps were generated (two-vs.-one, two-vs.-zero, and one-vs.-zero back).

Each contrast map was divided into 116 regions of interest (ROIs). For each ROI, the average beta contrast from each subject's *pre-season* was used to create confidence intervals (CIs) that would be used to test *in-season* and *post-season* scans. In contrast to earlier flagging work, density estimation was used to find the bounds of the CI.

Each contrast map was divided into 116 ROI's, with the region's value being its average contrast value. To estimate the possible range of values within a given region, the values from all players were grouped by ROI and were used in a kernel density

estimation. This density was then used to find the 95% CI's used to test the *in-season* and *post-season* values.

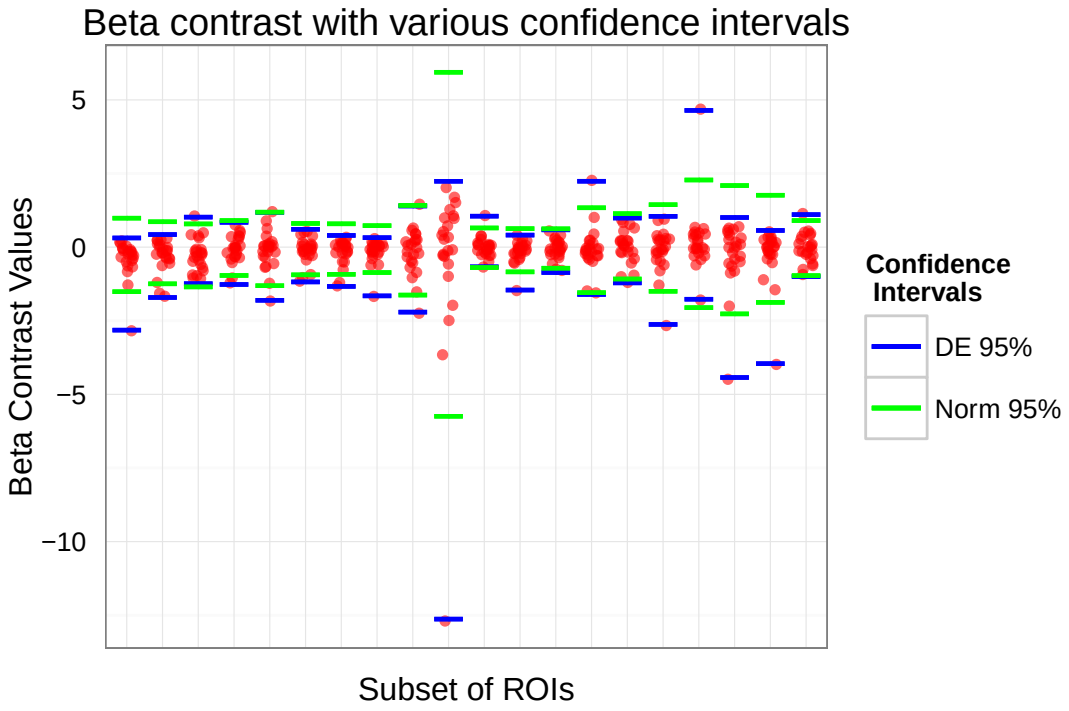

Fig. 3.1. This figures contrasts the new confidence intervals found using density estimate (DE) with those found using the normal distribution (Norm).

Figure 3.1 shows a subset of the CI's used in this analysis. Clearly, outliers will skew the subsequent analysis. Beyond the work presented by Shenk et al., an analysis was also done using only the ROI's with the smallest intervals, as they should represent the most consistent values [11]. However, the results matched very closely with those found using the full set of ROI's.

Using these confidence intervals, beta contrast values from *in-season* and *post-season* were tested. An ROI was flagged if the contrast value was outside of the CI. A player was flagged if twelve or more regions were flagged.

3.3 Results

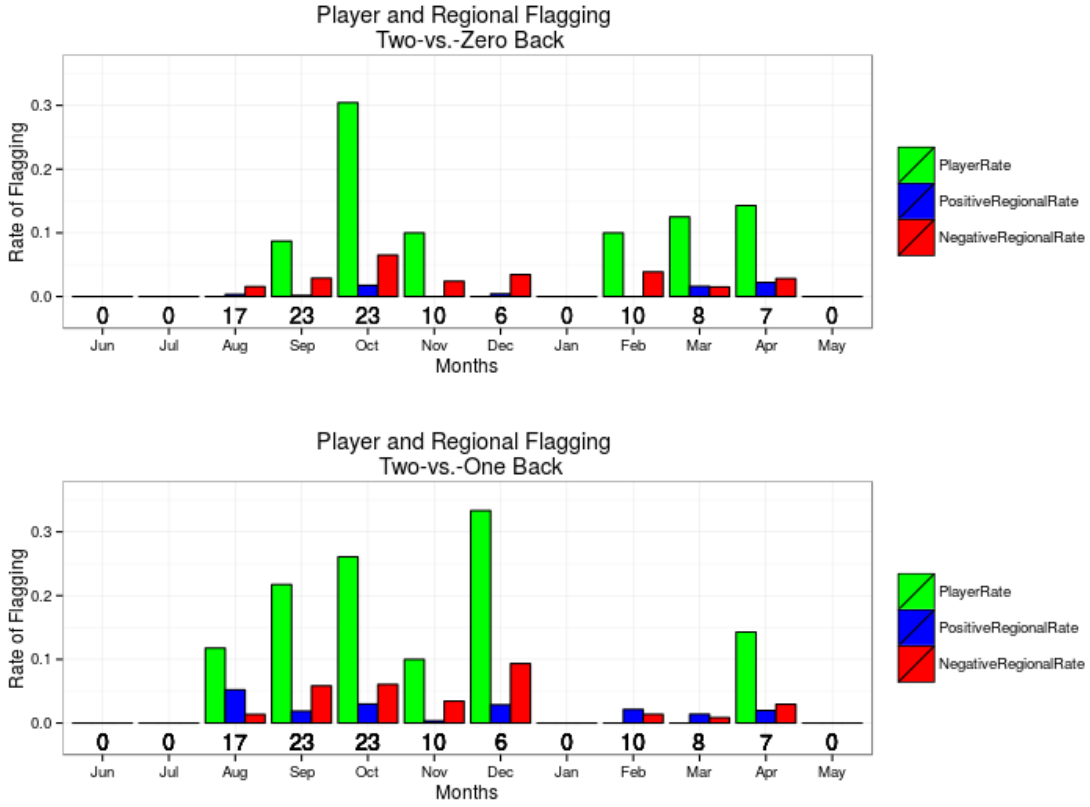

Fig. 3.2. Flagging rates for the two selected contrasts. The player rate is the ratio of players flagged to the total number of players tested. Regional rates are the ratio of the number of flagged regions over the total number of regions tested, where the total is the number of players in group times the number of regions per player. Positive and negative regional flagging refer to being above or below the confidence interval.

After initial exposure to contact, there is a large deviation in both contrasts. This deviation increased during the first several months before dropping near the end of the season. The flagging rates diminish following the cessation of contact in November and December.

The regional flagging rates show an interesting trend in the direction of flagging during the months of contact. There is a clear trend toward negative flagging rates

during the months of contact (August to November/December). A negative bias in the contrast could result from either decreased load needed for the more complex 2-back task or an increased load needed to complete the simpler 0-back or 1-back task. This flagging rate seems to normalize in the post-season scans.

3.4 Strengths and weaknesses of method

Weaknesses:

i) *There is not an obvious baseline for estimating the confidence intervals.*

Controls are needed to better estimate the confidence intervals. Both MRS and rsfMRI suggest that the contact athletes before the season already deviate from non-contact athletes. This would suggest some long term effect of contact and is most likely specific to the individual.

ii) *The task depends on subject cooperation.*

As is common to task-based fMRI, the results depend on the subject performing the task. If the subject loses concentration, the activations will no longer match with task presentation. There is also the issue that subjects may use different strategies for a single task. The use of line drawings was meant to discourage strategies that involved verbalizing the stimuli. [54], similarly, used fractals in a visual N-back task. His post interviews with the subject showed that participants still tried to verbalize the fractal drawings, though it was more difficult. The visual system would most likely be under a greater load, but visual memory may not be effectively probed.

iii) *It could be affected by exercise.*

Because of the nature of the BOLD signal, there could be short-term effects immediately after exercise or baseline differences as a result of consistent exercise. However, this would not be expected to be a significant confound to the current study. Football players generally participate in other sports outside of the

football season (e.g. swimming, track, cross-country, wrestling). Further, the subjects start conditioning practices before pre-season scans, so the observed changes should not be from transient changes from the onset of exercise.

Strengths:

i) *This method is very easy to compute and is straightforward.*

Once the contrast images have been generated, it takes little time to run all of this analysis.

ii) *It is conservative in the estimates of flagging.*

Kernel density estimation was used to decrease the false-positive rate of flagging. This method will be more robust for a skewed distribution. Also, outliers will significantly widen the confidence intervals.

ii) *The results can easily be combined with other methods.*

This method can give several outputs: number of flagged regions for a given player and a binary "player flagged" feature for each subject. This can be simply added to larger models to give a more complete picture of a subject.

3.5 Future direction

i) *Use controls to find a better baseline.*

Controls would provide a much better estimate of a healthy distribution than would the football players. Even in the *pre-season*, the contact history of some players could skew the distribution, resulting in misleading confidence intervals.

ii) *Parcellate the brain in a way that will be more robust for the given task.*

The parcellation used in the current study was not specific to the task but was based only on anatomic divisions. A better parcellation scheme would either group areas of similar activation or would group areas that show a low variance across subjects. An example two-vs.-zero back contrast is shown in Figure 3.3.

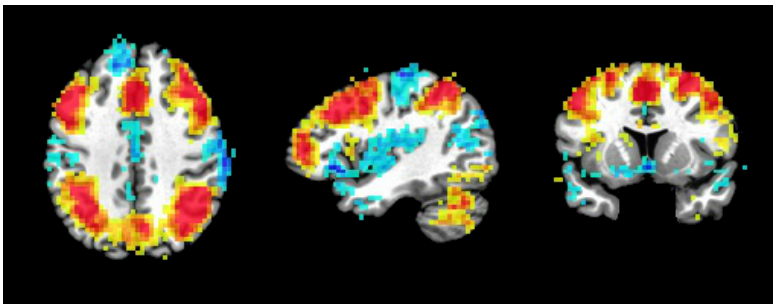

Fig. 3.3. Average two-vs.zero back contrast over forty-six *pre-season* scans. Warmer colors represent a positive bias towards the more complex two-back task. Cool colors show a bias towards the baseline zero-back task.

From Figure 3.3, it is clear that there are clear regions that are more active during the two-back task versus the zero-back. It would be reasonable have a parcellated the clearly active portions into groups. The other regions should still be included because functional reorganization could shift these contrasts.

Another way is to make parcels that are consistent across groups.

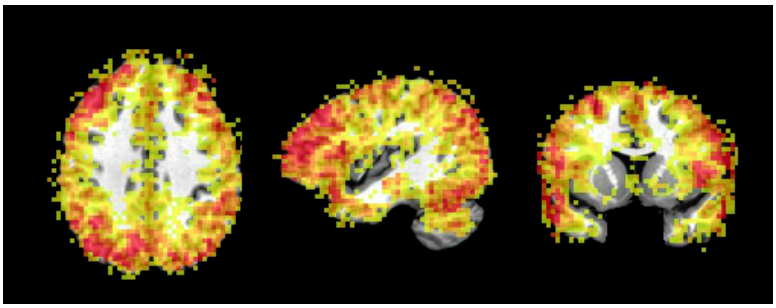

Fig. 3.4. Standard deviation of t-scores across the same forty-six subjects.

Figure 3.4 shows that regions that show a greater bias across players also show a larger standard deviation across the population. This would make parcellating based on consistency difficult and would favor those regions which do not show a bias.

A compromise could be a combination of the two, forming ROIs based on the level of activations while also trying to lower the ROI standard deviation across the group.

iii) *Use a combination of verbal and visual N-back tasks in a joint flagging metric.*

To reduce variance, an ensemble method could be used to combine different contrasts and tasks to make a more reliable flagging metric.

iv) *A model needs to be found that will connect the flagging results with some externally observable event.*

As mentioned in the introduction, a relationship should be found between hits and this measure.

4. ALTERATIONS FOUND IN HEMODYNAMIC RESPONSE OF HIGH SCHOOL FOOTBALL ATHLETES

4.1 Introduction

Involvement in high school sports has been steadily increasing, with 7.9 million students involved in sports in the 2015-16 playing year [55]. With sports participation

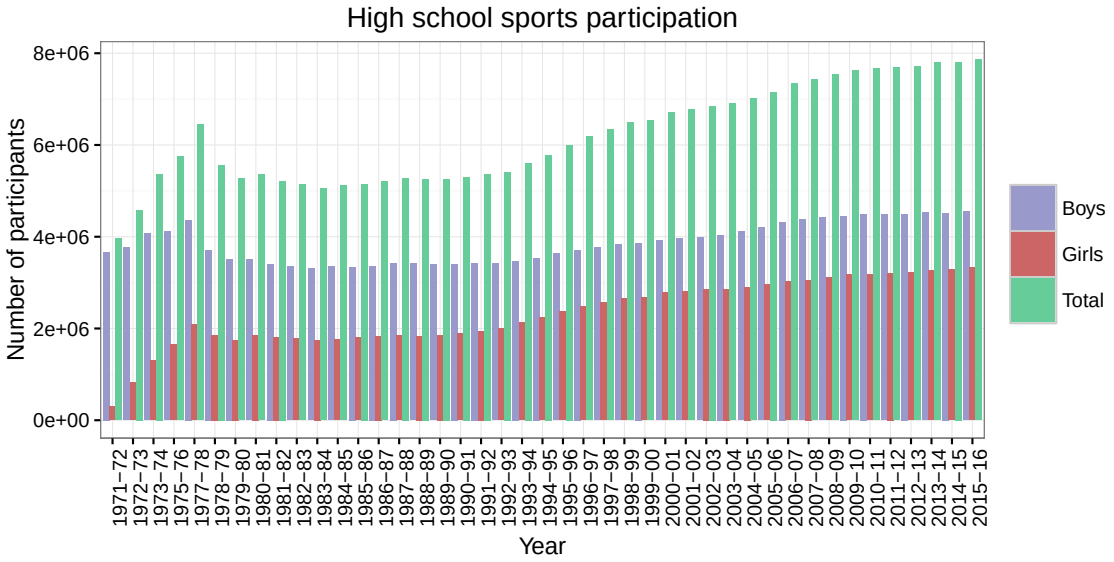

Fig. 4.1. Participation in high school sports.

comes the increased risk of injury, with an estimated 135,901 concussion occurring in the 2005-06 playing season as a result of this participation [56]. A concussion is a transient period of neurologic impairment due to mechanical insult to the head [15].

The transient nature of clinical symptoms has lead to the belief that the neural changes resulting from a concussion are also transient. However, there is mounting evidence that concussions can have a long lasting effect. Meehan et al. reported a

drop in quality of life in former collegiate athletes (aged 40-70 at the time of study) related to receiving a concussion while participating in sports in college [27]. In retired National Football League (NFL) players, Guskiewicz2007 et al. found that an increased risk of depression was linked to the number of concussions sustained during their athletic career [57]. Even more alarmingly, McKee et al. has reported a link to participation in professional football to chronic traumatic encephalopathy (CTE), a progressive neurodegenerative disease which clinically resembles Alzheimer's disease [3, 58]. High school athletes do not seem to understand the severity of concussions, with half of the athletes expressing the opinion that return to play should be somewhat dependent on the importance of a game or event to their team [59].

While some collision sport (e.g., football, wrestling, boxing) athletes experience a concussion, the vast majority of them regularly sustain subconcussive head acceleration events. The role of subconcussive events in increasing the risk for a more serious injury and in deteriorating long-term neural health is not yet known. McKee et al. and Gavett et al. reported cases of CTE that could not be linked to a player's previous history of concussion [3, 58]. In addition, cognitive scores in boxers have been shown to return to baseline control levels one month after a bout [60]. It is now being recognized that subconcussive events can have serious short-term and long-term effects [61].

Here we study the role of repetitive, subconcussive events in a population of high school football players. Specifically, the hemodynamic response (HDR) measured and tested for alterations in the course of a playing season. The HDR was chosen because of its linkage to blood flow and its prior study in the case of neuropathologies (e.g., schizophrenia, dementia, aging) [62, 63]. We are able to show that high school football athletes do show altered HDR curves in the first six weeks of the playing season. These changes diminish substantially as at the end of the season and after the season, suggesting a recovery (though not complete) to their subject specific baseline levels.

4.2 Materials and methods

4.2.1 Experimental design

During the scan session, there were nine presentations of a two-second, flashing checkerboard. Subjects were instructed to rapidly tap their fingers to their thumbs for the duration of the checkboard. Presentations of the stimulus were spaced 28-30 seconds apart.

4.2.2 Human subjects

During the 2012 year of the Purdue Neurotrauma Group's ongoing study, the HDR was measured. All subjects participated in high-school American football during this season. Subjects participated in one scanning session before the season (Pre, n=22), two during the season (In1, n=22; In2, n=20), and up to five after the season (Post1, n=10; Post2, n=11; Post1, n=11; Post4, n=10; Post5, n=10; Post6, n=18). The demanding logistics of the study allowed only a subset of the subjects to participate in five post-season scans, while the others have two post-season scans (referred to as Post1 and Post6 to match the time period of scans from subset).

4.2.3 Data aquisition

All imaging was performed using a 3T General Electric (Waukesha, WI) Signa HDx, located at the Purdue MRI Facility (West Lafayette, IN). All data were acquired with a 16-channel brain array (Nova Medical, Wilmington, MA). HDR scans (gradient-echo echo-planar sequence with scan length 5 min 30 sec; repetition time (TR) 500 ms; echo time (TE) 26 ms; flip angle 35; 10 slices at 2.5 mm; field of view 20 cm; 64 x 64 acquisition, resulting in 3.125 mm x 3.125 mm in-plane resolution) were acquired on all participants. A high-resolution T1-weighted anatomical was acquired for registration purposes using a three-dimensional spoiled gradient-recalled

echo sequence (TR 5.768 ms; TE 2.032 ms; flip angle 73; 0.9375 mm x 0.9375 mm x 1 mm).

4.2.4 Data preprocessing

Preprocessing of functional and structural data was performed using AFNI [64]. Structural images were registered to the MNI ICBM 2009 template [65, 66] using auto_warp.py, AFNI's nonlinear registration script. EPI scans were registered using the same warping applied to the structural scans.

The EPI scans were first time-shift corrected, then deobliqued using Fourier and quintic resampling, respectively. During deobliquing, voxels were resampled to be 2.5mm isotropic. The data then underwent despiking, linear alignment to structural, non-linear alignment to template, volume registered to the first TR, smoothing with a, isotropic filter with a 6mm FWHM, and voxel-wise time series scaling. Spatial smoothing was performed to reduce the effects of misregistration. Voxel time series were scaled to have an average of 100, allowing the regression weights to estimate the percent signal change.

It is worth noting that only a thin (25mm) oblique section of the brain was imaged. This compromise of partial coverage allowed for a TR of 0.5 seconds, giving finer quantification of the HDR. The operator had freedom to change the obliquity to ensure coverage of both visual cortex and primary motor. Misregistration can be a major concern for this type of scan, with small errors in the linear alignment leading to large errors in non-linear registration. Despite operator freedom and limited coverage, the intersubject and intersession overlap was very high, as is shown in Figure 4.2.

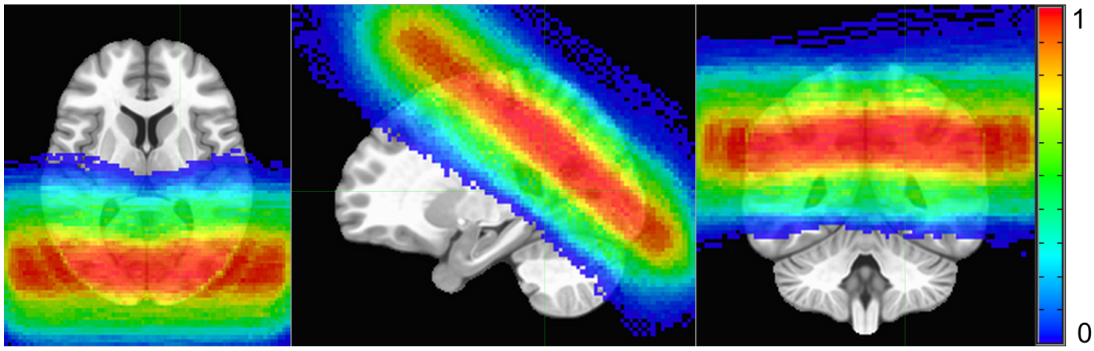

Fig. 4.2. Overlap of all registered EPI scans, with the MNI ICBM 2009 template as the base. A value of 1 refers to complete overlap.

4.2.5 Statistical modeling

Voxel time series were modeled using a GLM structure:

$$\mathbf{y} = \mathbf{X}\boldsymbol{\beta} + \boldsymbol{\epsilon} \tag{4.1}$$

Massive univariate analysis was performed using AFNI's 3dDeconvolve. The design matrix $\mathbf{X}$ is made up of tent regressors used to model the HDR, along with three Legendre polynomials to account for drift and six motion parameters (representing changes in orientation and translation). The HDR was modeled at each presentation as

$$r(t) = \sum_{i=1}^{19} \beta_i T(t-i) \tag{4.2}$$

where the inner tent functions are

$$T(t) = \begin{cases} 1 - |t|, & \text{for } |t| < 1 \\ 0 & \text{else} \end{cases} \tag{4.3}$$

The response $r(t)$ was discretized at with half second intervals to match the TR of the scan. Figure 4.3 shows the tent regressors used to estimate the HDR function as an finite impulse response (FIR) filter.

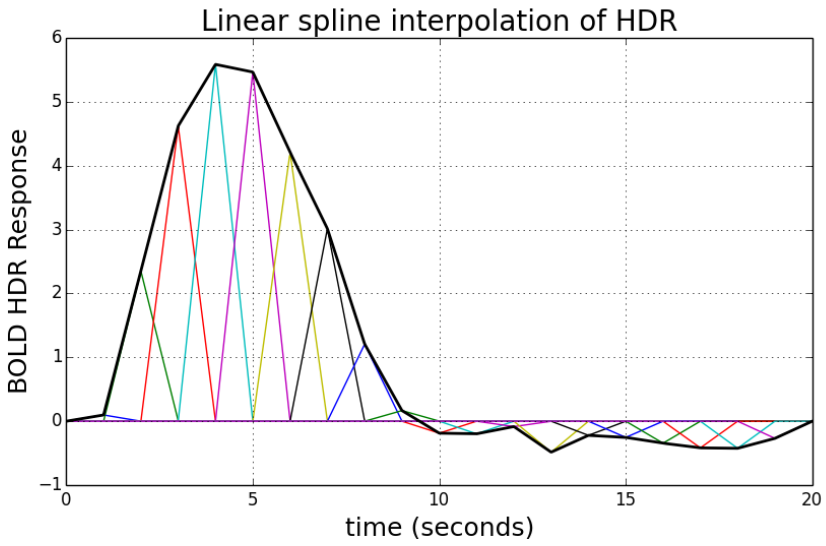

Fig. 4.3. Estimated HDR with associated tent functions.

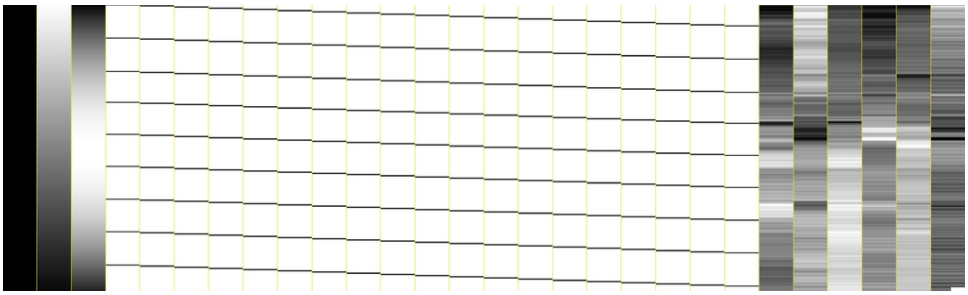

Fig. 4.4. Example full design matrix used in the regression analysis. The columns include three polynomials to handle drift, nineteen task regressors to estimate the HDR, and six motion parameters (three for orientation and three for translation in all three dimensions).

4.2.6 Statistical inference

Metrics tested in this analysis included the area under the curve (AUC) for the first ten seconds of activation, time-to-peak, and timecourse standard deviation. Paired *t*-

tests were performed using AFNI's 3dttest++ function, with their newly added (Feb 2016) clustsim option. This option will:

- Compute the residuals of the model at each voxel at the group level.
- Generate a null distribution by randomizing among subjects the signs of the residuals in the test, repeat the t-tests (with covariates, if present), and iterate 10,000 times.
- Take the 10,000 3D tstatistic maps from the randomization and use those as input to 3dClustSim (with no additional smoothing): threshold the maps, clusterize them, and then count the false positives.

[51]

This will first run a t-test, then calculate false alarm rates (FAR) for resulting clusters. More details about the cluster simulation can be found in Appendix A.2. The statistical analysis requires an appropriate mask (details of it can be found in Appendix A.3).

4.3 Results

A significant difference was found when comparing Pre with In1. A cluster (1477 voxels) in visual cortex showed a significant ($p << 0.01$) drop in AUC going from Pre to In1. The averaged response for these sessions is shown in Figure 4.5. A summary of the results can be found in Table 4.1.

No difference in the time-to-peak was observed for any session compared to Pre. When comparing timecourse variance, one weakly significant cluster (62 voxels, voxelwise $p < 0.01$, cluster $p < 0.04$) was observed at In1 in the visual cortex, indicating a decrease in variance. No other significant clusters were found.

Session compared to Pre	**Significant clusters (voxel $p < 0.01$, cluster $p < 0.05$)**
In1 (n=22)	Negative, **1477** voxels ($p << 0.01$), secondary visual
	Positive, 359 voxels ($p < 0.02$), right motor
	Negative, 326 voxels ($p < 0.03$), central motor
In2 (n=20)	None
Post1 (n=10)	None
Post2 (n=11)	Negative, 96 voxels ($p < 0.05$), right visual
Post3 (n=10)	Positive, 213 voxels ($p < 0.01$), left motor
	Positive, 161 voxels ($p < 0.02$), right motor
Post4 (n=10)	Negative, 96 voxels ($p < 0.04$), left motor
Post5 (n=10)	Negative, 81 voxels ($p < 0.04$), left motor
Post6 (n=18)	Negative, 185 voxels ($p < 0.02$), left motor

Table 4.1
Summary of results from the AUC analysis. A negative cluster indicates a reduction in AUC when comparing to Pre.

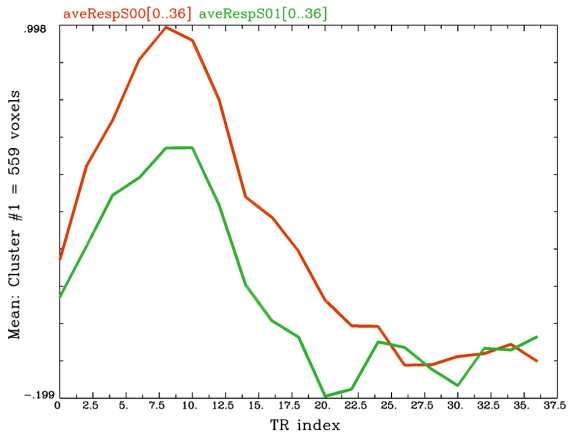

Fig. 4.5. Average time series within the significant cluster for sessions Pre and In1. Notice that Pre>In1. On the x-axis, each TR is 0.5 seconds and the zeroth TR corresponds to one second after stimulus presentation.

4.4 Discussion

Several types of changes could be driving the decrease in the HDR AUC going from Pre to In1:

1. Shifts in area of functional involvement
2. Decreased ability to signal for increased delivery of glucose/oxygen
3. Decreased ability of the vasculature to respond to energy needs

Changes to the area of functional involvement were not specifically tested. However, the mask used for testing was generated using Pre and In1 scans, therefore a shift would most likely be accompanied by positive and negative clusters in the visual region.

Buckner et al. found a similar change in a study on young adults, and demented and nondemented older adults [63]. That study found a decrease in HDR amplitude in older adults (both demented and nondemented) compared to young adults, as shown in Figure 4.6. As in the current study, they were not able to be certain of the cause of this decrease.

This direction could also suggest that the region is in a hypometabolic state. As discussed in Chapter 2, an occurrence of mTBI is first followed by a short period of hypermetabolism, then a longer period of hypometabolism. This hypometabolism is considered to be a period of increased vulnerability to further injury. The subjects in the current study did not experience the symptoms of a concussion that would related to hypermetabolism (loss of consciousness, confusion, amnesia). In the absence of a concussion, perhaps repetitive subconcussive trauma is sufficient to drive a state of vulnerability as the brain adjusts to a marked increase in mechanical stresses.

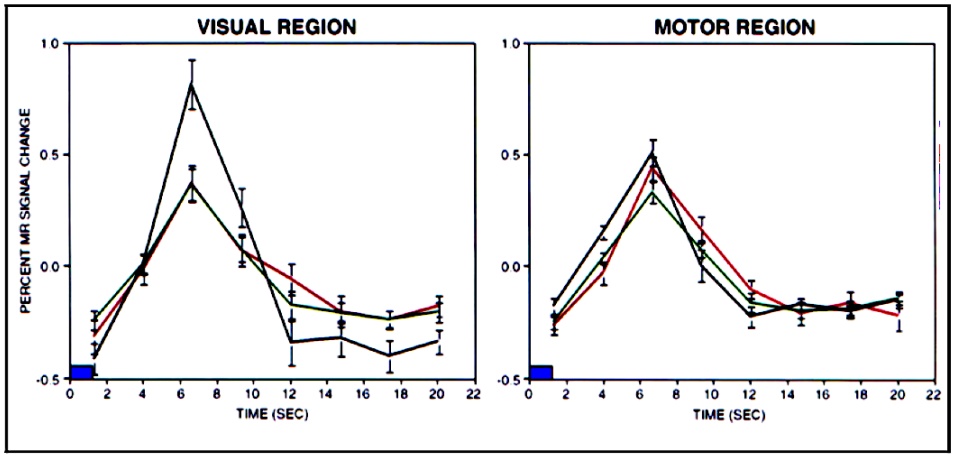

Fig. 4.6. Average responses from the visual and motor cortex. [63] The young adult group (black line) showed higher amplitudes compared to the both the demented (red) and nondemented (green) older adult groups in the visual region, but not in the motor region.

5. DUAL REGRESSION RESTING STATE ANALYSIS

5.1 Background of dual regression

ICA has emerged as one of the most popular methods used to study resting state networks (RSNs). ICA (using a specified number of components) has been shown to give consistent results when applied to groups. However, when testing for group differences, individual component time series and spatial maps are needed. One method, first outlined by Filippini et al., to generate subject-specific measurements is dual regression [67]. The analysis includes:

1. Temporally concatenating all scans, perform an ICA to separate network temporal dynamics and spatial maps. This corresponds to solving the equation

$$Y_g = \beta_g X_g + E \tag{5.1}$$

   where Y_g is the temporal concatenation of all individual scans, β_g contains the group component spatial maps, and X_g contains the component time courses. Both β_g and X_g are unknown and must be estimated. Several group spatial maps are shown in 5.1.

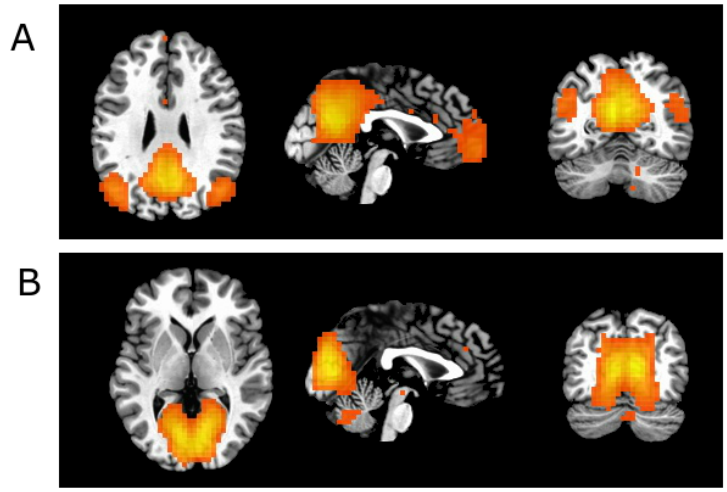

Fig. 5.1. Two examples networks extracted using a twenty component ICA on soccer *pre-season* (n=15) and control (n=14) athletes. The pictures networks are the DMN (A) and the medial visual network (B).

2. Back project the group spatial maps on the individual scans to produce subject specific timecourses. This solves the equation

$$Y_i = \beta_g X_i + E \tag{5.2}$$

Where Y_i is an individual's scan and X_i is an individual's component time series related to the group spatial maps. Because Y_i and β_g are known, X_i can be solved for by simply using OLS.

3. Use subject specific time series to create subject specific spatial maps. This step solves

$$Y_i = \beta_i X_i + E \tag{5.3}$$

Where β_i are the individual spatial maps. As in the previous step, β_i can be solved using OLS because Y_i and X_i are known.

Four subject specific maps from the DMN are shown in 5.2.

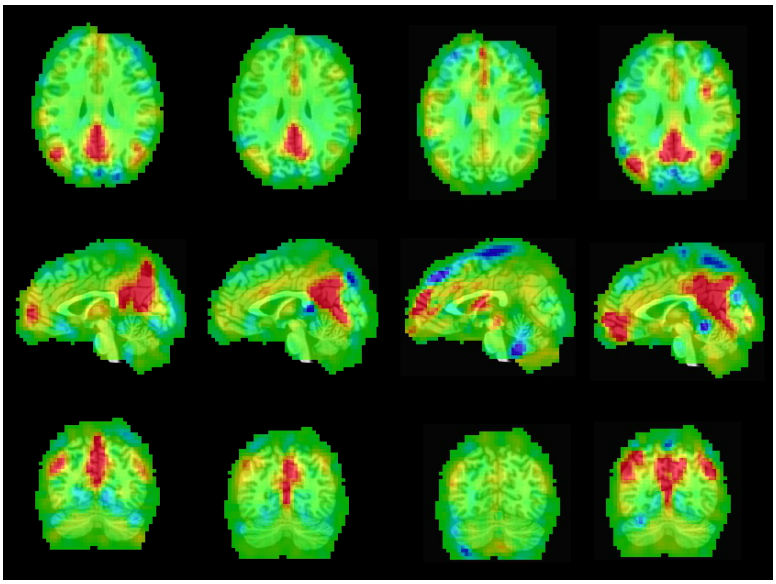

Fig. 5.2. Three example individual specific DMN's found during dual-regression.

4. Test for group difference using a randomization test, as described by [68].

5.2 Current study

5.2.1 Materials and Methods

Human subjects

Subjects were recruited from two high-school girl's soccer teams. Subjects participated in one scanning session before the season (Pre, n=27), two during the season (In1, n=16; In2, n=17), and two after the season (Post1, n=16; Post2, n=16).

In addition to soccer players, controls were also recruited from girl's non-contact sports teams. They underwent an initial scan (n=14) and a follow-up (n=14) which was used to assess measurement reliability.

Data aquisition

All imaging was performed using a 3T General Electric (Waukesha, WI) Signa HDx, located at the Purdue MRI Facility (West Lafayette, IN). All data were acquired with a 16-channel brain array (Nova Medical, Wilmington, MA). Resting state scans (gradient-echo echo-planar sequence with scan length 9 min 48 sec; repetition time (TR) 2000 ms; echo time (TE) 26 ms; flip angle 35; 34 slices at 3.8 mm; field of view 20 cm; 64 x 64 acquisition, resulting in 3.125 mm x 3.125 mm in-plane resolution) were acquired on all participants. A high resolution T1-weighted anatomical was acquired for registration purposes using a three-dimensional spoiled gradient-recalled echo sequence (TR 5.768 ms; TE 2.032 ms; flip angle 73; 0.9375 mm x 0.9375 mm x 1 mm).

Data preprocessing

Resting state scans were preprocessed using FSL's FEAT tool. Processing included volume registration, spatial smoothing (5mm FWHM Gaussian kernel), high pass temporal smoothing, exploratory ICA (number of components were automatically estimated for each subject), and registration to the MNI ICBM 2009 template. Further denoising was performed using FSL's FIX (FMRIB's ICA-based Xnoiseifier) [69, 70]. Dual regression was also performed using FSL's dual_regression script.

5.2.2 Quality of dual regression output

In a slight variation of the method described in Section 5.1, this study did not use a group ICA generated from the temporal concatenation of all subject scans. Instead, the maps used by Smith et al., which the authors made publicly available, were used as templates [40]. This was done to avoid the possible dangers of "double dipping" [71]. Also, using the templates should make the results more generalizable:

anyone with resting state data (many datasets are now publicly available) and with the Smith et al. template should be able to perform a comparable study.

To see if the networks were well represented following dual regression, each individual spatial map was correlated with its corresponding template map (Figure 5.3).

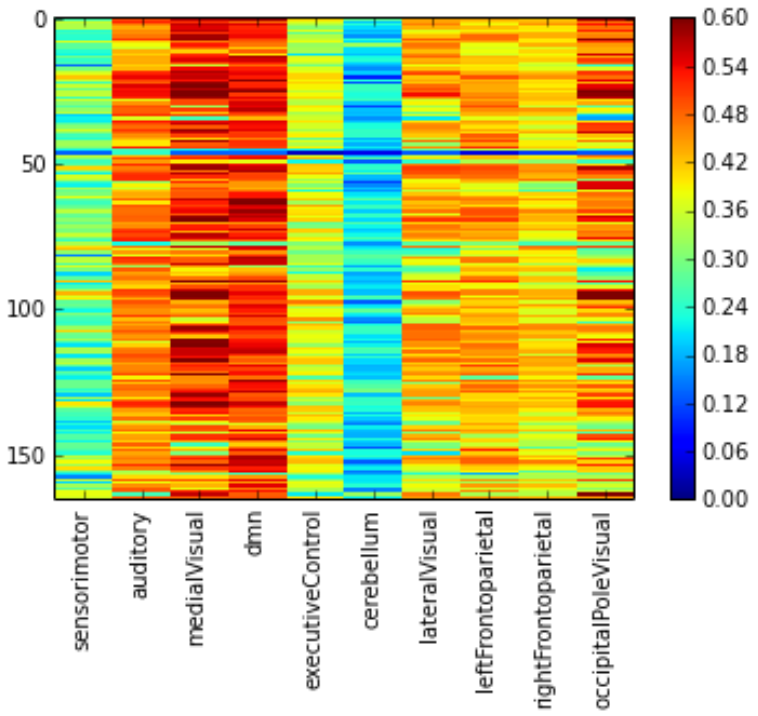

Fig. 5.3. Each row represents a single subject, with each column being the different networks. The color of each entry represents the spatial correlation coefficient of that subject's network with the group template. Apart from cerebellum and sensorimotor, the networks showed good correlation to the template.

As seen in Figure 5.3, cerebellum and sensorimotor are not reliably present following dual regression. This is to be expected for the cerebellum, as the imaging protocol did not generally capture the entire cerebellum. It is less clear why sensorimotor is poorly correlated with the template. Sensorimotor is near the edge of the brain dorsally and may have been somewhat masked during analysis. Perhaps a less

stringent mask is needed for this (AFNI now recommends calculating most preliminary statistics before applying a mask, as blurring and spatial normalization often lead to true activations appearing outside of the brain).

Overall, this is a promising amount of agreement between the subject specific maps and the template. Few subjects (approximately two) exhibited poor correlation across all networks. As a metric of subject-scan quality, the the rows of Figure 5.3 were averaged and plotted (Figure 5.4).

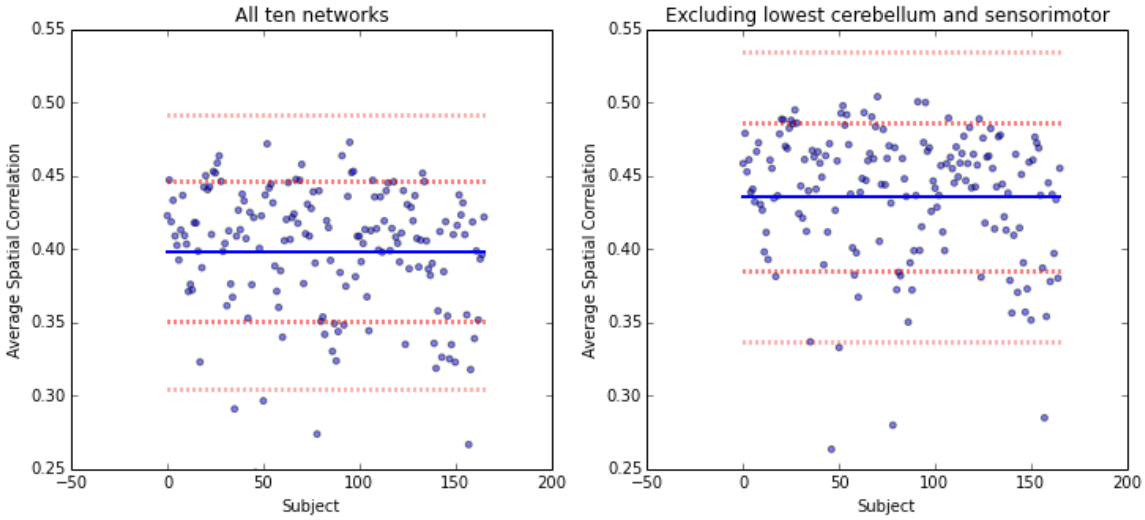

Fig. 5.4. Each point shows the average spatial correlation of networks with the template across subjects. This is equivalent to averaging the rows of Figure 5.3. A high value means that the subject's networks were well represented by the output of dual regression. The left plot is an average of all ten networks, while the right excludes the two lowest networks, cerebellum and sensorimotor.

5.2.3 Internetwork correlations

The correlation between networks is seen as either a way of sharing information or as a form of activity modulation. Time courses for each of the networks were pairwise correlated using a lag-optimization method. This performs circular shifts of the data and take the maximum resulting correlation coefficient. The justification here is

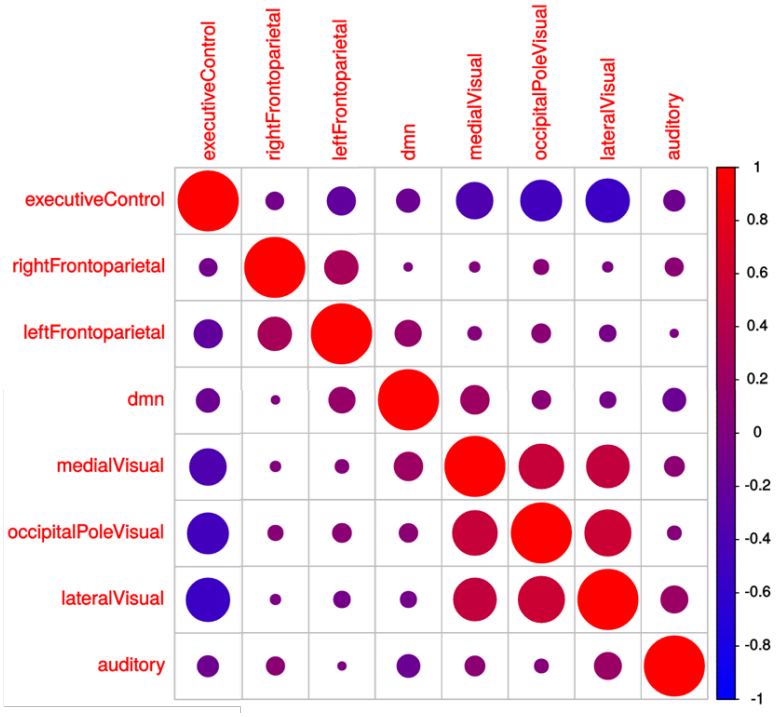

Fig. 5.5. This represents the correlation of each pair of component time course (the correlations are averaged across subjects). The absolute strength of the correlation is represented by the size of the dot, with the strength and direction represented by the color.

that the metric of interest is how similar the time courses are between components regardless of a time shift (as the time shift could be viewed as signal propagation time). This internetwork correlation has been studied in relation to aging, depression, schizophrenia, and other conditions [72–74]. Figure 5.5 is the average correlation between the ten networks in the current study.

The correlation coefficient was transformed for further analysis. The metric of interest was

$$z = \operatorname{arctanh}(|\rho|) \tag{5.4}$$

Simply taking $\operatorname{arctanh}(\rho)$ is also a reasonable choice. The absolute value was taken in this study because it was only the amount of correlation that was of interest (the amount of temporal similarity), rather than the phase of the signals.

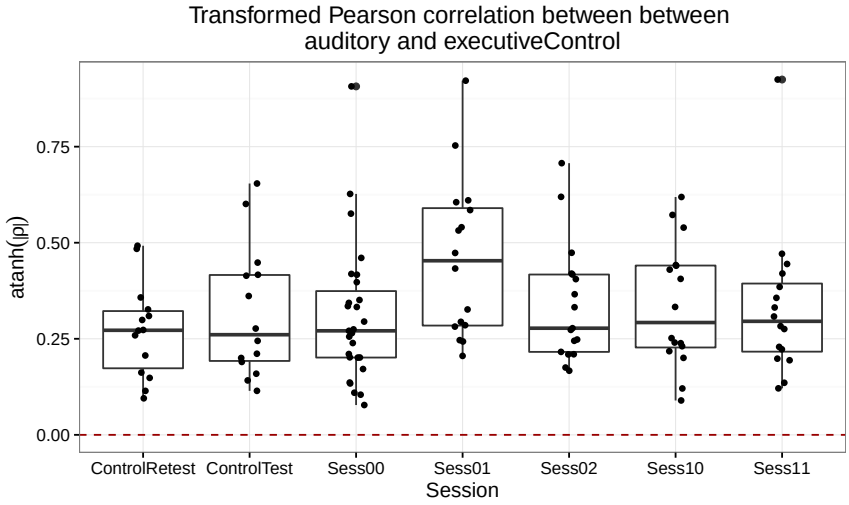

Fig. 5.6. Example of a particular network pair that seems to show a change. Notice that the control's test and retest sessions appear to be comparable, only the player In1 is changed in these sessions.

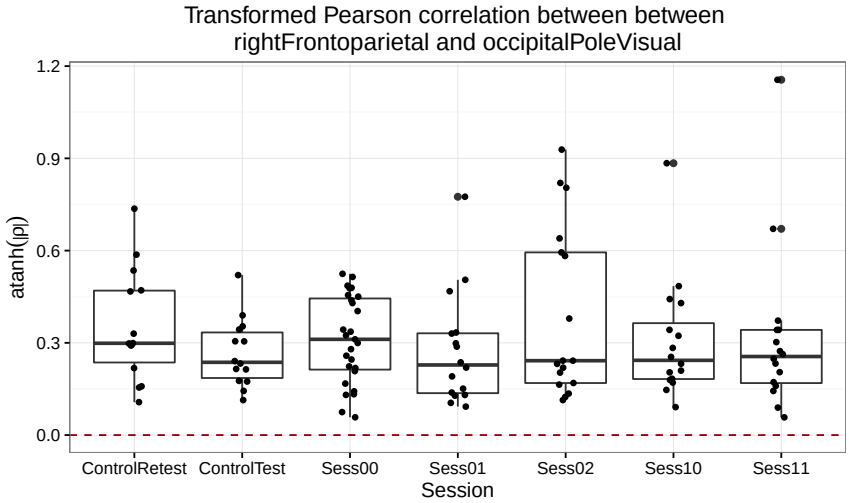

Fig. 5.7. Another network pair, but this does not show any noticeable pattern.

Figures 5.6 and 5.7 show two examples of the internetwork correlation of a network pair during the season. Figure 5.6 shows what appears to be a shift in correlation

from the Pre to In1 scans, with a return to Pre levels in the remaining scans. It is interesting that this is observed at the In1 session, as this appears to be a consistent trend across different modalities and methods in the study [6, 8, 11]. However, it may be unwise to rely too heavily on this internetwork correlation, as the evidence is very weak. It is possible that a different preprocessing method or statistical analysis will yield more significant results, but little can be inferred at this point, as there are many connections that look like Figure 5.7 with no particular pattern.

5.3 Future work

ICA-based methods, such as dual regression, have shown promise detecting disorders. The current study has been able to accurately reproduce resting state networks using a publicly available template and extract several metrics of interest. More work is needed to see if there is a relationship of these measures to recorded impacts. It is possible that a multivariate approach may be more fruitful, where multiple kinds of measures are used simultaneously. The benefit of looking at the metrics individually, as was done here, is that interpretation of the results is much easier. However, if the effect size is too small and the noise is too high, more data may need to be pooled to show differences between groups.

Another possible measurement to take from these components is the power signal density (PSD) of the component time courses. This was briefly looked at, with some methods outlined in Appendix B.2.

The quality of the scans could also be improved through the use of better noise reduction methods. ICA-based methods are showing promise in removing the noise due to motion and physiology. FSL's FIX was used for in the current study, which must be trained to find noise components. There is a new option, AROMA (Automatic Reduction of Motion Artifacts), that uses theoretical results of noise characterization, and therefore does not need to be trained [75].

6. CONCLUSIONS AND FUTURE WORK

6.1 Summary of findings

Using advanced imaging techniques, this work has demonstrated neural changes in athletes during the course of a playing season. The hemodynamic response task exhibited a reduced AUC, meaning a possible reduction in cerebral blood flow or in local neural energy consumption. The visual task showed altered activation levels, with the predominant trend being a decrease in the observered contrast (both two-vs-zero and two-vs-one), suggesting the brain must work harder to perform a simple task. Both of these measurements, taken in separate seasons and with different players, show a marked change after the first six weeks of the contact play. This gives evidence that a change in the rate of exposure can have a drastic effect on neural function. Notably, these changes happen in the absence of clinical symptoms. These findings, along with other work from the Purdue Neurotrauma Group, suggest that neural injury can result from subconcussive impacts, despite the player's lack of clinical symptoms.

6.2 Future work

More work is needed to refine the measurements being used and connect them with head impact data. The addition of quantitative measurements of cerebral blood flow or cerebral metabolic rate of oxygen could provide valuable insight into the mechanisms of injury. After reliable MRI measurements are found, the next step is to connect them with impact data. One goal of this would be to create a predictive model of risk or injury as a function of hits exposure. Most likely, hits exposure would itself be a function of several factors, including number of impacts, severity of

impacts (such as metrics of linear and angular acceleration), and rate of exposure. The Purdue Neurotrauma Group, with its extensive dataset (spanning eight years of data collection as of 2016), is in a unique position to build such a model. The validation of an accurate model would be invaluable to the athletic community, as it would enable intelligent management of risk (both short- and long-term) in a way that has not been possible before.

LIST OF REFERENCES

LIST OF REFERENCES

[1] M. Marar, N. M. McIlvain, S. K. Fields, and R. D. Comstock, "Epidemiology of concussions among united states high school athletes in 20 sports," *The American journal of sports medicine*, vol. 40, no. 4, pp. 747–755, 2012.

[2] D. K. Menon, K. Schwab, D. W. Wright, A. I. Maas, *et al.*, "Position statement: definition of traumatic brain injury," *Archives of physical medicine and rehabilitation*, vol. 91, no. 11, pp. 1637–1640, 2010.

[3] A. C. McKee, R. C. Cantu, C. J. Nowinski, E. T. Hedley-Whyte, B. E. Gavett, A. E. Budson, V. E. Santini, H.-S. Lee, C. A. Kubilus, and R. A. Stern, "Chronic traumatic encephalopathy in athletes: progressive tauopathy following repetitive head injury," *Journal of neuropathology and experimental neurology*, vol. 68, no. 7, p. 709, 2009.

[4] C. M. Baugh, J. M. Stamm, D. O. Riley, B. E. Gavett, M. E. Shenton, A. Lin, C. J. Nowinski, R. C. Cantu, A. C. McKee, and R. A. Stern, "Chronic traumatic encephalopathy: neurodegeneration following repetitive concussive and subconcussive brain trauma," *Brain imaging and behavior*, vol. 6, no. 2, pp. 244–254, 2012.

[5] K. Abbas, T. Shenk, V. Poole, M. Robinson, L. Leverenz, E. Nauman, and T. Talavage, "Effects of repetitive sub-concussive brain injury on the functional connectivity of default mode network in high school football athletes," *Developmental Neuropsychology*, vol. 40, no. 01, pp. 51–56, 2015.

[6] K. Abbas, T. E. Shenk, V. N. Poole, E. L. Breedlove, L. J. Leverenz, E. A. Nauman, T. M. Talavage, and M. E. Robinson, "Alteration of default mode network in high school football athletes due to repetitive subconcussive mild traumatic brain injury: a resting-state functional magnetic resonance imaging study," *Brain connectivity*, vol. 5, no. 2, pp. 91–101, 2015.

[7] E. L. Breedlove, M. Robinson, T. M. Talavage, K. E. Morigaki, U. Yoruk, K. O'Keefe, J. King, L. J. Leverenz, J. W. Gilger, and E. A. Nauman, "Biomechanical correlates of symptomatic and asymptomatic neurophysiological impairment in high school football," *Journal of biomechanics*, vol. 45, no. 7, pp. 1265–1272, 2012.

[8] V. N. Poole, K. Abbas, T. E. Shenk, E. L. Breedlove, K. M. Breedlove, M. E. Robinson, L. J. Leverenz, E. A. Nauman, T. M. Talavage, and U. Dydak, "Mr spectroscopic evidence of brain injury in the non-diagnosed collision sport athlete," *Developmental neuropsychology*, vol. 39, no. 6, pp. 459–473, 2014.

[9] V. Poole, E. Breedlove, T. Shenk, K. Abbas, M. Robinson, L. Leverenz, E. Nauman, U. Dydak, and T. Talavage, "Sub-concussive hit characteristics predict deviant brain metabolism in football athletes," *Developmental Neuropsychology*, vol. 40, no. 01, pp. 12–17, 2015.

[10] M. Robinson, T. Shenk, E. Breedlove, L. Leverenz, E. Nauman, and T. Talavage, "The role of location of subconcussive head impacts in fmri brain activation change," *Developmental Neuropsychology*, 2015.

[11] T. Shenk, M. Robinson, D. Svaldi, K. Abbas, K. Breedlove, L. Leverenz, E. Nauman, and T. Talavage, "fmri of visual working memory in high school football players," *Developmental Neuropsychology*, 2015.

[12] D. Svaldi, C. Joshi, M. Robinson, K. Abbas, T. Shenk, E. Nauman, L. Leverenz, and T. Talavage, "Cerebrovascular reactivity alterations in asymptomatic high school football players," *Developmental Neuropsychology*, 2015.

[13] M. Faul, L. Xu, M. M. Wald, and V. Coronado, "Traumatic brain injury in the united states," *Atlanta, GA: national Center for injury Prevention and Control, Centers for disease Control and Prevention*, 2010.

[14] E. Finkelstein, P. S. Corso, and T. R. Miller, *The incidence and economic burden of injuries in the United States*. Oxford University Press, USA, 2006.

[15] P. McCrory, W. H. Meeuwisse, M. Aubry, B. Cantu, J. Dvořák, R. J. Echemendia, L. Engebretsen, K. Johnston, J. S. Kutcher, M. Raftery, *et al.*, "Consensus statement on concussion in sport: the 4th international conference on concussion in sport held in zurich, november 2012," *British journal of sports medicine*, vol. 47, no. 5, pp. 250–258, 2013.

[16] B. Willer and J. J. Leddy, "Management of concussion and post-concussion syndrome," *Current Treatment Options in Neurology*, vol. 8, no. 5, pp. 415–426, 2006.

[17] C. C. Giza and D. A. Hovda, "The neurometabolic cascade of concussion," *Journal of athletic training*, vol. 36, no. 3, p. 228, 2001.

[18] C. C. Giza and D. A. Hovda, "Ionic and metabolic consequences of concussion," *Neurologic Athletic Head and Spine Injuries. Philadelphia, PA: WB Saunders*, pp. 80–100, 2000.

[19] S. Signoretti, G. Lazzarino, B. Tavazzi, and R. Vagnozzi, "The pathophysiology of concussion," *PM&R*, vol. 3, no. 10, pp. S359–S368, 2011.

[20] A. Ommaya, W. Goldsmith, and L. Thibault, "Biomechanics and neuropathology of adult and paediatric head injury," *British journal of neurosurgery*, vol. 16, no. 3, pp. 220–242, 2002.

[21] T. Walilko, D. C. Viano, and C. A. Bir, "Biomechanics of the head for olympic boxer punches to the face," *British journal of sports medicine*, vol. 39, no. 10, pp. 710–719, 2005.

[22] H. S. Levin, H. M. Eisenberg, and A. L. Benton, *Mild head injury*. Oxford University Press, 1989.

[23] A. Yoshino, D. A. Hovda, T. Kawamata, Y. Katayama, and D. P. Becker, "Dynamic changes in local cerebral glucose utilization following cerebral concussion in rats: evidence of a hyper-and subsequent hypometabolic state," *Brain research*, vol. 561, no. 1, pp. 106–119, 1991.

[24] L. Longhi, K. E. Saatman, S. Fujimoto, R. Raghupathi, D. F. Meaney, J. Davis, A. McMillan, V. Conte, H. L. Laurer, S. Stein, *et al.*, "Temporal window of vulnerability to repetitive experimental concussive brain injury," *Neurosurgery*, vol. 56, no. 2, pp. 364–374, 2005.

[25] H. L. Laurer, F. M. Bareyre, V. M. Lee, J. Q. Trojanowski, L. Longhi, R. Hoover, K. E. Saatman, R. Raghupathi, S. Hoshino, M. S. Grady, *et al.*, "Mild head injury increasing the brain's vulnerability to a second concussive impact," *Journal of neurosurgery*, vol. 95, no. 5, pp. 859–870, 2001.

[26] M. Field, M. W. Collins, M. R. Lovell, and J. Maroon, "Does age play a role in recovery from sports-related concussion? a comparison of high school and collegiate athletes," *The Journal of pediatrics*, vol. 142, no. 5, pp. 546–553, 2003.

[27] W. P. Meehan III, A. M. Taylor, P. Berkner, N. J. Sandstrom, M. W. Peluso, M. M. Kurtz, A. Pascual-Leone, and R. Mannix, "Division iii collision sports are not associated with neurobehavioral quality of life," *Journal of neurotrauma*, vol. 33, no. 2, pp. 254–259, 2016.

[28] S. P. Broglio, J. T. Eckner, H. L. Paulson, and J. S. Kutcher, "Cognitive decline and aging: the role of concussive and subconcussive impacts," *Exercise and sport sciences reviews*, vol. 40, no. 3, p. 138, 2012.

[29] S.-G. Kim and P. A. Bandettini, "Principles of functional mri," in *BOLD fMRI: A guide to functional imaging for neuroscientists* (S. H. Faro and F. B. Mohamed, eds.), Springer Science & Business Media, 2010.

[30] P. W. Stroman, *Essentials of functional MRI*. CRC Press, 2011.

[31] S. Ogawa, T.-M. Lee, A. S. Nayak, and P. Glynn, "Oxygenation-sensitive contrast in magnetic resonance image of rodent brain at high magnetic fields," *Magnetic resonance in medicine*, vol. 14, no. 1, pp. 68–78, 1990.

[32] R. B. Buxton, E. C. Wong, and L. R. Frank, "Dynamics of blood flow and oxygenation changes during brain activation: the balloon model," *Magnetic resonance in medicine*, vol. 39, no. 6, pp. 855–864, 1998.

[33] R. B. Buxton, "Dynamic models of bold contrast," *Neuroimage*, vol. 62, no. 2, pp. 953–961, 2012.

[34] A. M. Dale and R. L. Buckner, "Selective averaging of rapidly presented individual trials using fmri," *Human brain mapping*, vol. 5, no. 5, pp. 329–340, 1997.

[35] P. A. Bandettini, E. C. Wong, R. S. Hinks, R. S. Tikofsky, and J. S. Hyde, "Time course epi of human brain function during task activation," *Magnetic Resonance in Medicine*, vol. 25, no. 2, pp. 390–397, 1992.

[36] N. K. Logothetis, "The underpinnings of the bold functional magnetic resonance imaging signal," *The Journal of Neuroscience*, vol. 23, no. 10, pp. 3963–3971, 2003.

[37] K. J. Friston, A. P. Holmes, K. J. Worsley, J.-P. Poline, C. D. Frith, and R. S. Frackowiak, "Statistical parametric maps in functional imaging: a general linear approach," *Human brain mapping*, vol. 2, no. 4, pp. 189–210, 1994.

[38] S. M. Smith and T. E. Nichols, "Threshold-free cluster enhancement: addressing problems of smoothing, threshold dependence and localisation in cluster inference," *Neuroimage*, vol. 44, no. 1, pp. 83–98, 2009.

[39] M. D. Fox and M. E. Raichle, "Spontaneous fluctuation in brain activity observed with functional magnetic resonance imaging," *Nature*, vol. 8, pp. 700–711, 2007.

[40] S. M. Smith, P. T. Fox, K. L. Miller, D. C. Glahn, P. M. Fox, C. E. Mackay, N. Filippini, K. E. Watkins, R. Toro, A. R. Laird, *et al.*, "Correspondence of the brain's functional architecture during activation and rest," *Proceedings of the National Academy of Sciences*, vol. 106, no. 31, pp. 13040–13045, 2009.

[41] A. Hyvärinen and E. Oja, "Independent component analysis: algorithms and applications," *Neural networks*, vol. 13, no. 4, pp. 411–430, 2000.

[42] C. F. Beckmann and S. M. Smith, "Probabilistic independent component analysis for functional magnetic resonance imaging," *Medical Imaging, IEEE Transactions on*, vol. 23, no. 2, pp. 137–152, 2004.

[43] S. Chen, T. J. Ross, W. Zhan, C. S. Myers, K.-S. Chuang, S. J. Heishman, E. A. Stein, and Y. Yang, "Group independent component analysis reveals consistent resting-state networks across multiple sessions," *Brain research*, vol. 1239, pp. 141–151, 2008.

[44] C. F. Beckmann, M. DeLuca, J. T. Devlin, and S. M. Smith, "Investigations into resting-state connectivity using independent component analysis," *Philosophical Transactions of the Royal Society of London B: Biological Sciences*, vol. 360, no. 1457, pp. 1001–1013, 2005.

[45] J. Damoiseaux, S. Rombouts, F. Barkhof, P. Scheltens, C. Stam, S. M. Smith, and C. Beckmann, "Consistent resting-state networks across healthy subjects," *Proceedings of the national academy of sciences*, vol. 103, no. 37, pp. 13848–13853, 2006.

[46] M. Iacoboni, J. Freedman, J. Kaplan, K. H. Jamieson, T. Freedman, B. Knapp, and K. Fitzgerald, "This is your brain on politics," *New York Times*, vol. 11, pp. 1–2, 2007.

[47] A. Aron, D. Badre, M. Brett, J. Cacioppo, C. Chambers, R. Cools, S. Engel, M. DEsposito, C. Frith, E. Harmon-Jones, *et al.*, "Politics and the brain," *New York Times*, vol. 14, 2007.

[48] Z. Yang, Z. Huang, J. Gonzalez-Castillo, R. Dai, G. Northoff, and P. Bandettini, "Using fmri to decode true thoughts independent of intention to conceal," *NeuroImage*, vol. 99, pp. 80–92, 2014.

[49] C. M. Bennett, M. Miller, and G. Wolford, "Neural correlates of interspecies perspective taking in the post-mortem atlantic salmon: An argument for multiple comparisons correction," *Neuroimage*, vol. 47, no. Suppl 1, p. S125, 2009.

[50] A. Eklund, T. E. Nichols, and H. Knutsson, "Cluster failure: Why fmri inferences for spatial extent have inflated false-positive rates," *Proceedings of the National Academy of Sciences*, p. 201602413, 2016.

[51] R. W. Cox, R. C. Reynolds, and P. A. Taylor, "Afni and clustering: False positive rates redux," *bioRxiv*, p. 065862, 2016.

[52] A. M. Owen, K. M. McMillan, A. R. Laird, and E. Bullmore, "N-back working memory paradigm: A meta-analysis of normative functional neuroimaging studies," *Human brain mapping*, vol. 25, no. 1, pp. 46–59, 2005.

[53] M. Robinson, E. Breedlove, V. Poole, L. Leverenz, E. Nauman, and T. Talavage, "Proximal and distal effects of subconcussive head impacts on fmri activity in asymptomatic high school football players." 2013 meeting of the International Society for Magnetic Resonance Imaging, 2013.

[54] J. D. Ragland, B. I. Turetsky, R. C. Gur, F. Gunning-Dixon, T. Turner, L. Schroeder, R. Chan, and R. E. Gur, "Working memory for complex figures: an fmri comparison of letter and fractal n-back tasks.," *Neuropsychology*, vol. 16, no. 3, p. 370, 2002.

[55] N. F. of State High School Associations, "2015-16 high school athletics participation survey," dec 2016.

[56] L. M. Gessel, C. L. Collins, and R. W. Dick, "Concussions among united states high school and collegiate athletes," *Journal of athletic training*, vol. 42, no. 4, p. 495, 2007.

[57] K. M. Guskiewicz, S. W. Marshall, J. Bailes, M. McCrea, H. P. Harding, A. Matthews, J. R. Mihalik, and R. C. Cantu, "Recurrent concussion and risk of depression in retired professional football players," *Medicine and science in sports and exercise*, vol. 39, no. 6, p. 903, 2007.

[58] B. E. Gavett, R. A. Stern, R. C. Cantu, C. J. Nowinski, and A. C. McKee, "Mild traumatic brain injury: a risk factor for neurodegeneration," *Alzheimer's research & therapy*, vol. 2, no. 3, p. 1, 2010.

[59] T. L. Miyashita, E. Diakogeorgiou, B. Hellstrom, N. Kuchwara, E. Tafoya, and L. Young, "High school athletes perceptions of concussion," *Orthopaedic journal of sports medicine*, vol. 2, no. 11, p. 2325967114554549, 2014.

[60] L. D. Ravdin, W. B. Barr, B. Jordan, W. E. Lathan, and N. R. Relkin, "Assessment of cognitive recovery following sports related head trauma in boxers," *Clinical Journal of Sport Medicine*, vol. 13, no. 1, pp. 21–27, 2003.

[61] J. E. Bailes, A. L. Petraglia, B. I. Omalu, E. Nauman, and T. Talavage, "Role of subconcussion in repetitive mild traumatic brain injury: a review," *Journal of neurosurgery*, vol. 119, no. 5, pp. 1235–1245, 2013.

[62] J. M. Ford, M. B. Johnson, S. L. Whitfield, W. O. Faustman, and D. H. Mathalon, "Delayed hemodynamic responses in schizophrenia," *Neuroimage*, vol. 26, no. 3, pp. 922–931, 2005.

[63] R. L. Buckner, A. Z. Snyder, A. L. Sanders, M. E. Raichle, and J. C. Morris, "Functional brain imaging of young, nondemented, and demented older adults," 2006.

[64] R. W. Cox, "Afni: software for analysis and visualization of functional magnetic resonance neuroimages," *Computers and Biomedical research*, vol. 29, no. 3, pp. 162–173, 1996.

[65] V. S. Fonov, A. C. Evans, R. C. McKinstry, C. Almli, and D. Collins, "Unbiased nonlinear average age-appropriate brain templates from birth to adulthood," *NeuroImage*, vol. 47, p. S102, 2009.

[66] V. Fonov, A. C. Evans, K. Botteron, C. R. Almli, R. C. McKinstry, D. L. Collins, B. D. C. Group, *et al.*, "Unbiased average age-appropriate atlases for pediatric studies," *NeuroImage*, vol. 54, no. 1, pp. 313–327, 2011.

[67] N. Filippini, B. J. MacIntosh, M. G. Hough, G. M. Goodwin, G. B. Frisoni, S. M. Smith, P. M. Matthews, C. F. Beckmann, and C. E. Mackay, "Distinct patterns of brain activity in young carriers of the apoe-ε4 allele," *Proceedings of the National Academy of Sciences*, vol. 106, no. 17, p. 7209, 2009.

[68] T. E. Nichols and A. P. Holmes, "Nonparametric permutation tests for functional neuroimaging: a primer with examples," *Human brain mapping*, vol. 15, no. 1, pp. 1–25, 2002.

[69] L. Griffanti, G. Salimi-Khorshidi, C. F. Beckmann, E. J. Auerbach, G. Douaud, C. E. Sexton, E. Zsoldos, K. P. Ebmeier, N. Filippini, C. E. Mackay, *et al.*, "Ica-based artefact removal and accelerated fmri acquisition for improved resting state network imaging," *Neuroimage*, vol. 95, pp. 232–247, 2014.

[70] G. Salimi-Khorshidi, G. Douaud, C. F. Beckmann, M. F. Glasser, L. Griffanti, and S. M. Smith, "Automatic denoising of functional mri data: combining independent component analysis and hierarchical fusion of classifiers," *Neuroimage*, vol. 90, pp. 449–468, 2014.

[71] N. Kriegeskorte, W. K. Simmons, P. S. Bellgowan, and C. I. Baker, "Circular analysis in systems neuroscience: the dangers of double dipping," *Nature neuroscience*, vol. 12, no. 5, pp. 535–540, 2009.

[72] K. Onoda, M. Ishihara, and S. Yamaguchi, "Decreased functional connectivity by aging is associated with cognitive decline," *Journal of cognitive neuroscience*, vol. 24, no. 11, pp. 2186–2198, 2012.

[73] A. Manoliu, C. Meng, F. Brandl, A. Doll, M. Tahmasian, M. Scherr, D. Schwerthöffer, C. Zimmer, H. Förstl, J. Bäuml, *et al.*, "Insular dysfunction within the salience network is associated with severity of symptoms and aberrant inter-network connectivity in major depressive disorder," *Frontiers in human neuroscience*, vol. 7, p. 930, 2014.

[74] A. Manoliu, V. Riedl, A. Zherdin, M. Mühlau, D. Schwerthöffer, M. Scherr, H. Peters, C. Zimmer, H. Förstl, J. Bäuml, *et al.*, "Aberrant dependence of default mode/central executive network interactions on anterior insular salience network activity in schizophrenia," *Schizophrenia bulletin*, p. sbt037, 2013.

[75] R. H. Pruim, M. Mennes, D. van Rooij, A. Llera, J. K. Buitelaar, and C. F. Beckmann, "Ica-aroma: a robust ica-based strategy for removing motion artifacts from fmri data," *Neuroimage*, vol. 112, pp. 267–277, 2015.

APPENDIX

A. CHAPTER 4 NOTES

A.1 Preprocessing scripts

A.1.1 Time shift correction and deobliquing

Deobliquing is necessary for this preprocessing. It's important to note that time-shift correction must be performed *before* deobliquing. Time shift correction must be performed on the original slices, therefore deobliquing first will results in incorrect shifts. AFNI guards against this by setting a flag in the header after deobliquing so that time-shift correction will not be run. However, it is up to the researcher to see this and apply the correct steps, as there is no error generated by not time-shifting, only a warning that the dataset has already be shifted.

Below is the code used to perform time-shift correction and deobliquing. The input is the original, oblique, EPI dataset.

```
1 #!/bin/bash
2
3 workingFile=${1/.HEAD/}
4 wD=$(dirname $1)
5
6 3dTshift -Fourier -prefix $wD/hdr.ts.nii.gz $workingFile
7 3dWarp -deoblique -quintic -newgrid 2.5              \
8        -prefix $wD/hdr.ts.deob.nii.gz               \
9        $wD/hdr.ts.nii.gz
```

A.1.2 Main preprocessing step

The main preprocessing takes a significant amount of time to run. Though many commands run will use multiple cores, the system still may not be fully utilized. One way to help is to use GNU's parallel function as a job manager. This can be easily set up by opening a new screen

```
screen -S parallel
```

and then running the command

```
true >jobqueue; tail -n+0 -f jobqueue | parallel --joblog logfile -j 8
```

Press `Ctl+a`, then `d` to detach the screen. Now jobs can be submitted to the queue by appending the jobqueue file. The tail command will watch the file for changes and send new lines to parallel. This particular command will run eight jobs in parallel. The time to process any one particular player session will be increased because it must share the CPU time with other jobs, but the system will be nearly fully utilized, resulting in significant overall time reduction compared to running the processes serially.

Most of the processing is done by calling AFNI's `afni_proc.py` script. Using this script for the bulk of the work makes it simpler for others to reproduce the research. The script below finds all football player's S00 and S01 from season 4 and 5, then sends a preprocessing command to the job queue for each player session. This script assumes the directories have names such as `Y4_P0204_S00`.

```
#!/bin/bash

topDir=$(pwd)
for i in $(ls -d Y[45]_P[01]*S0[01]| sort); do
  echo "cd $topDir/$i; \
  mkdir /trey/processedHDR_v3/$i;
  cd /trey/processedHDR_v3/$i;
  afni_proc.py -subj_id $i \
 -dsets $(pwd)/$i/hdr.ts.deob.nii.gz \
 -out_dir /trey/processedHDR_v3/$i/$i.tentHDR.results \
 -copy_anat /trey/warpedAnatomicals/$i/awpy/anat.ns.nii \
 -blocks despike align tlrc volreg mask blur scale regress \
 -tlrc_base /trey/warpedAnatomicals/$i/awpy/base.nii* \
 -volreg_align_e2a \
 -blur_size 6 \
 -align_opts_aea -cost lpc+ZZ \
 -anat_has_skull no \
 -volreg_tlrc_warp \
 -volreg_interp -Fourier \
 -tlrc_NL_warp \
 -tlrc_NL_warped_dsets /trey/warpedAnatomicals/$i/awpy/anat.un.aff.qw.nii \
                       /trey/warpedAnatomicals/$i/awpy/anat.un.aff.Xat.1D \
                       /trey/warpedAnatomicals/$i/awpy/anat.un.aff.qw_WARP.nii \
 -tlrc_NL_awpy_rm yes \
 -tcat_remove_first_trs 10 \
 -regress_stim_times_offset -5 \
 -regress_stim_times /trey/AcmeLab/processedHDR/hdrStim.1D \
 -regress_basis  'TENT(1,19,19)' \
 -regress_apply_mot_types demean deriv\
 -regress_censor_motion 0.3 \
 -regress_censor_outliers 0.1 \
 -regress_compute_fitts  \
 -regress_opts_3dD -TR_times 1 \
 -regress_reml_exec \
 -regress_run_clustsim no \
 -remove_preproc_files \
 -scr_overwrite \
 -execute" >> ~/jobqueue
done
cd $topDir
```

A.2 Cluster Simulation

AFNI's cluster simulation is a method to calculate measures of significance while making few assumptions about the distribution of the data. The resulting table is a table of $Pr(\text{“cluster size”} > \text{“given size”}|H_0,\ u_c)$, where the null hypothesis H_0 is that there are no active voxels and u_c is the cluster-forming threshold. The cluster-forming threshold is the t-statistic corresponding to p-values ranging from 0.0001 to 0.05.

The first step in this procedure is to calculate the voxel-wise statistics from the original data. In the current context, that is done by performing a one-sample t-test on the data. Each voxel is assumed to follow the linear model

$$y = \beta + e \tag{A.1}$$

and each voxel's t-stat is

$$t = \frac{\hat{\beta}}{S}\sqrt{N} \tag{A.2}$$

where N is the total number of subjects, and S is the sample standard deviation, which is given by

$$S = \sqrt{\frac{\sum(\hat{\beta} - \bar{\beta})^2}{N-1}} \tag{A.3}$$

and $\hat{\beta}$ is our current estimate (in the HDR study, that could mean AUC, time-to-peak, or time-course variance).

This will form a statistical map, T. Clustering is performed on the map after applying the threshold u_c. This particular study used first-nearest-neighbors (voxels had to share a face to form a cluster).

To generate a null distribution, each voxel was replaced with the residual from the test

$$r = y - \hat{\beta} \tag{A.4}$$

This corresponds to the null hypothesis that $\beta = 0$.

Sign flipping was performed on each subject's residual image.

$$R = \{R_0, R_1, \ldots, R_{N-1}\} \tag{A.5}$$

$$R^* = \{\pi_0 R_0, \pi_1 R_1, \ldots, \pi_{N-1} R_{N-1}\} \tag{A.6}$$

Where R_i is the i^{th} subject's residual map, π_i is the sign flipping variable with $Pr(\pi_i = 1) = Pr(\pi_i = -1) = 0.5$, and R^* is the set of sign-flipped residual images. Flipping the entire image preserves the spatial characteristics of the original image. Voxel-wise t-testing and clustering is then performed on the set of sign-flipped residuals in the same way as mentioned above. Cluster sizes are saved for the set of values of u_c. This processed is repeated 10,000 times to generate $m^*(n, u_c)$, the number of clusters found of size n at threshold u_c across all iterations of the null datasets.

Finally, to get an α for the i^{th} observed cluster of size n_i, it is simply a matter of calculating

$$\alpha = \frac{1}{M} \sum_{n_k > n_i} m^*(n_k, u_c) \tag{A.7}$$

where $M = \sum_{i=1}^{\infty} m^*(i, u_c)$, the total number of clusters found.

While this method avoids the pitfalls of distribution assumptions inherent in parametric models, it makes the assumption that a single statistical threshold is sufficient for the entire map. This is certainly false and results in differing false positive rates across the image.

A.3 Mask creation

A mask was needed to select the regions which were active during each two-second presentation of the flashing checkerboard. Initially, a t-test was performed on the maximum value from the first ten seconds of each response curve. Taking the maximum allowed the voxels with much noise to dominate. Inspection of the time series showed that the mask did not appropriately take well-defined time-series.

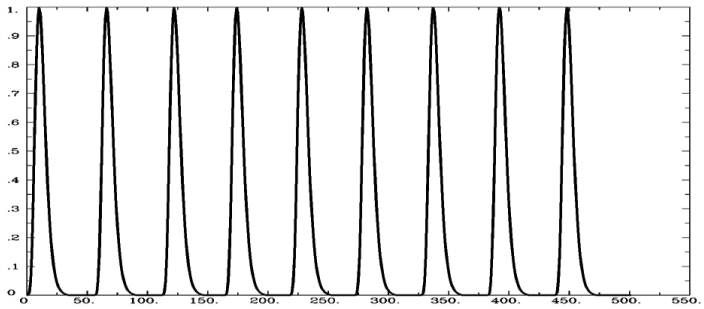

Fig. A.1. Stimulus regressor used when performing fixed-shaped regression.

A better mask was found by doing a standard block regression with the regressor shown in Figure A.1. A t-test on the resulting β coefficients did seem to extract those regions which had a clear HDR signal.

A.4 Effect of motion

Further analysis was done to see if a subject's motion had a residual effect on the quality of scans. To test this, a group activation map was generated using AFNI's 3dttest++ and then spatially correlated with the individual maps that went into the group. A low or negative correlation means that the individual scan does not have the same spatial pattern compared to the group. In this study, that could mean that there is a disruption in the functional networks due to repetitive head trauma, but it could also be due to unaddressed noise sources.

A group spatial map from the two-back task is shown in Figure A.2. This is made from 636 scans. Nuisance motion regressors for this map included six regressors to capture translation and rotation and their six derivatives. All preprocessing was performed in AFNI similar to what is described in Appendix A.1.2.

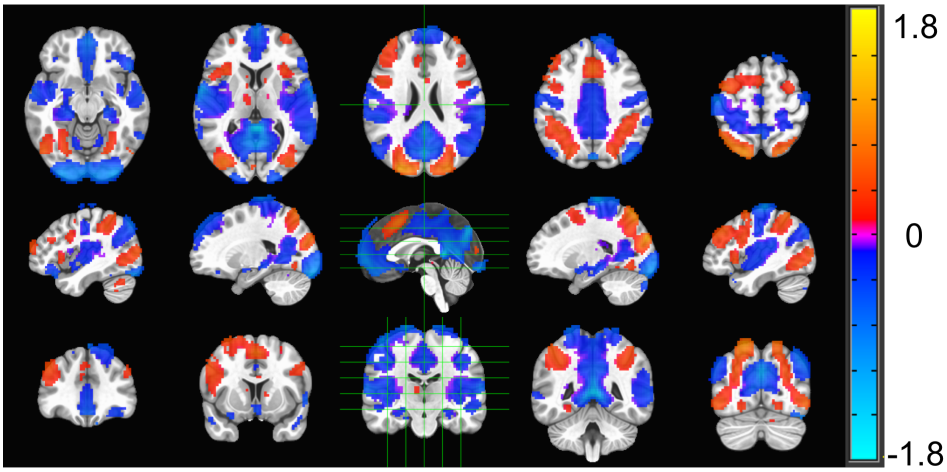

Fig. A.2. Group map (n=636) from two back task. The map is thresholded by the t-statistic at the 75th-percentile point ($p_{\text{uncorrected}} = 5e-19$, $q = 1e-15$). The β coefficient is represented by the color and is in arbitrary units of percent signal change.

There is a heavy skew in the distribution of the motion. The histogram of the average motion per TR is shown in Figure A.3.

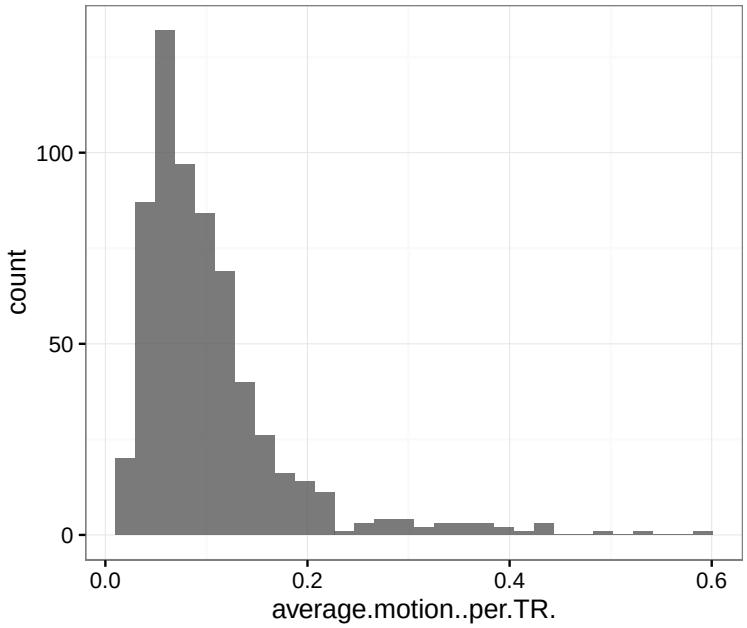

Fig. A.3. Histogram of average motion per TR. Notice that there is a very heavy skew to this distribution.

The distribution appears much more Gaussian after applying a log10 tranformation (Figure A.4). A simple regression of spatial correlation with average motion per TR is very significant ($p < 2.2e - 16$), but only has an $R^2 = 0.14$ (see Figure A.5).

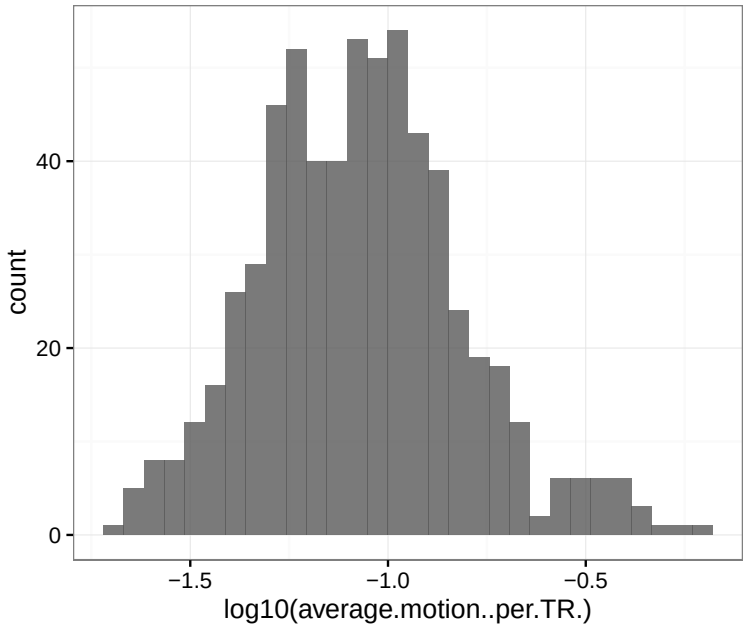

Fig. A.4. Histogram of log10(average motion per TR). Notice that there is much less skew after the transformation.

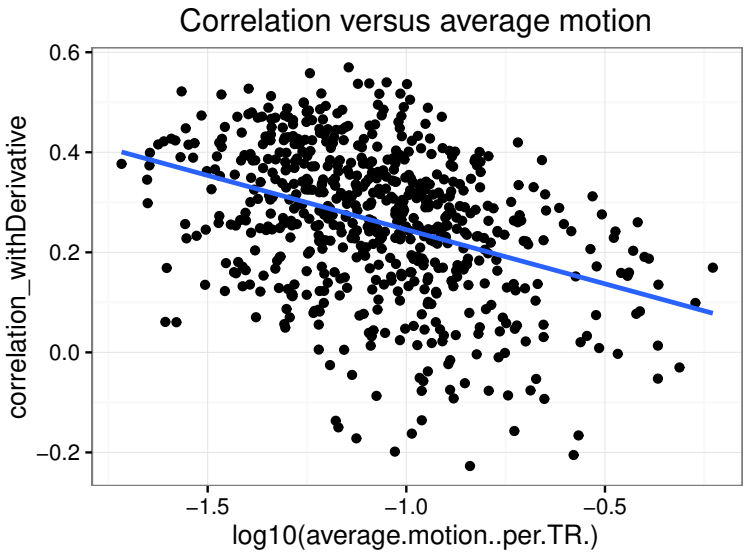

Fig. A.5. Stimulus regressor used when performing fixed-shaped regression.

The motion derivatives are often used as additional regressors to remove extra noise variance. To test how effective this was in the current dataset, a group map was made from the mean of all two-back maps, both with (n=632) and without (n=636) motion derivatives. This map was then correlated with each individual map and the results were plotted against each other, as shown in Figure A.6. It should be noted that a paired t-test did show a significant difference between the two methods ($p = 3.81e-05$) with the average correlation coefficient being 0.006 higher while not using the motion derivatives. Though this is a significant difference, the effect size is essentially small enough to ignore.

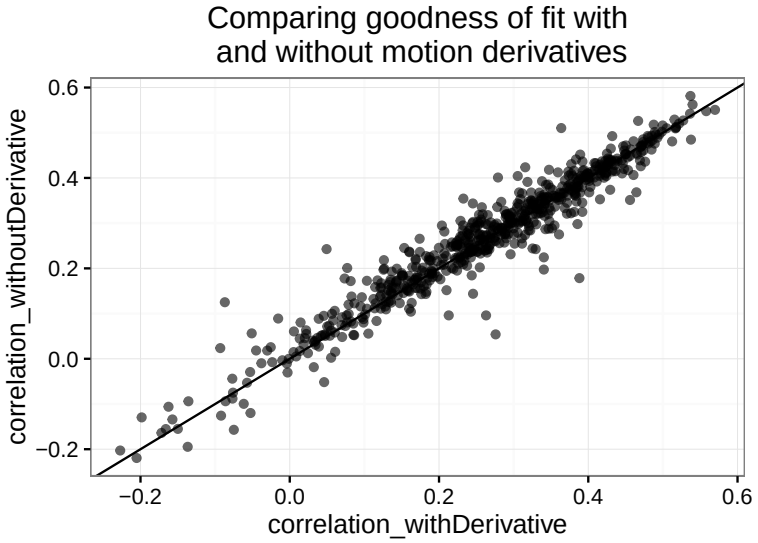

Fig. A.6. Goodness-of-fit, in this case, is defined as the spatial correlation to the group mask. There is little difference between the two methods. Plotted line is slope=1, intercept=0 (not a regression line from the data).

B. CHAPTER 5 NOTES

B.1 Disappearing results

A preliminary finding, which was presented at the 2015 meeting of the Biomedical Engineering Society, showed a significant, large-scale result. It showed a large disruption in the executive control network of high school soccer players compared to controls (see Figure B.1).

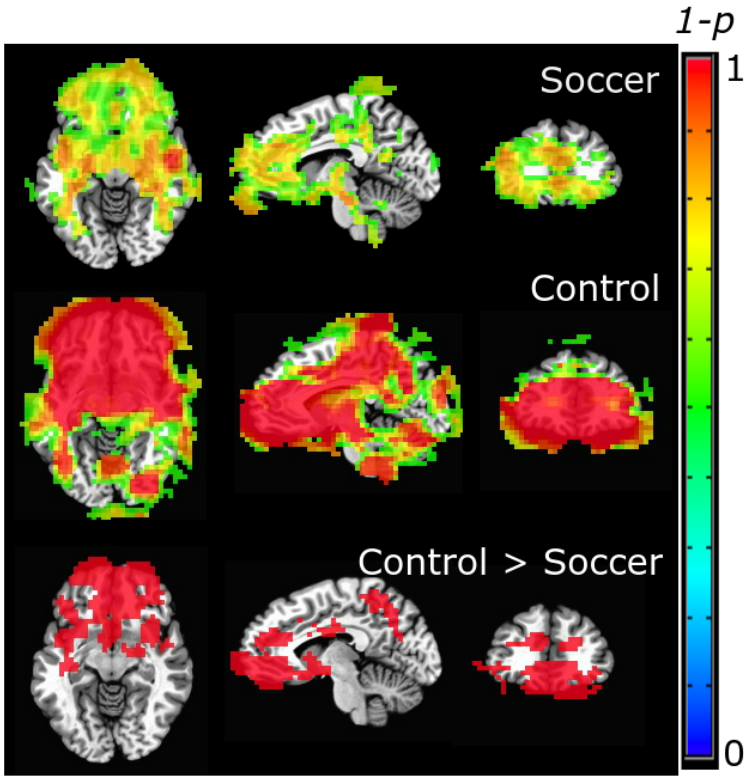

Fig. B.1. Results of permutation tests, with warmer colors representing higher certainty that the network is present in the given regions. Shown are the soccer players in their first *in-season* (top row), female controls (middle row), and test of controls greater than players.

It is interesting that the difference appeared only in the first in-season scan. This pattern (a difference appearing soon after the start of contact play) is consistent with other findings by the Purdue Neurotrauma Group. However, there was very little cleaning of the data when these results were made, limited mainly to volume registration, time-shift correction, and high-pass filtering. This was done because of a misunderstanding of the methods recommended for this dual regression procedure. In general, minimally processed data can be given to ICA (like FSL's MELODIC) and the algorithm will accurately separate noise and signal sources. Dual regression does not have that characteristic. As it is simply a two-step regression, it cannot separate noise sources from true signal. As a result, there was certainly a large degree of noise still present in the data, despite the promising resulting spatial maps.

When the misunderstanding was discovered, much effort was made to accurately clean the data and reproduce the results. Processing was done using FSL's FEAT, followed by FIX (FMRIB's ICA-based Xnoiseifier, a stretch of an acronym). [69, 70] After this additional cleaning, no significant results were found.

It may seem unusual that such a large difference in only one session could be due to noise. One could even argue that the noise must have been structured in order for this to happen, particularly since it fit well with other results from the same lab. But one could also argue that large false-positives are exactly what would be expected in a study like this. Studies with limited subjects and high levels of noise are more prone to large deviations. In the absence of proper data cleaning, the unusually large amounts of noise in this limited dataset would make it much more likely that a false-positive would also have a large effect size.

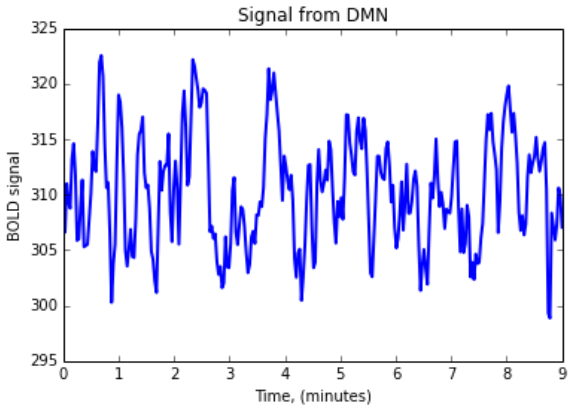

Fig. B.2. Example component time course for the DMN.

B.2 Power spectral density

Performing dual regression results in subject level time courses and spatial maps. An example of a DMN time course is shown in Figure B.2. Statistical analysis can be performed on the spectral properties these time courses. The estimated PSD of the signal shown in Figure B.2 is shown in Figure B.3. Further, the PSD of DMN timecourses from all subjects were taken and averaged (Figure B.4).

One issue with this method is the number of parameters involved in the calculation. Using Welch's method, the window function, segment length, segment overlap, length of FFT, and type of detrending can be chosen. More work needs to be done to find the proper parameters which will result in test-retest reliability.

Once the PSD is found, another measurement is the amplitude of low-frequency fluctuations (ALFF) or the fraction amplitude of low-frequency fluctuations (fALFF). ALFF can be defined as

$$\text{ALFF} = \int_0^{f_c} P_{xx}(f)df \tag{B.1}$$

Where P_{xx} is the PSD of interest and f_c is the cutoff for low frequencies. One reasonable choice is $f_c = 0.8$Hz. Then fALFF can be defined as

$$\text{fALFF} = \frac{\int_0^{f_c} P_{xx}(f)df}{\int_0^{\infty} P_{xx}(f)df} \tag{B.2}$$

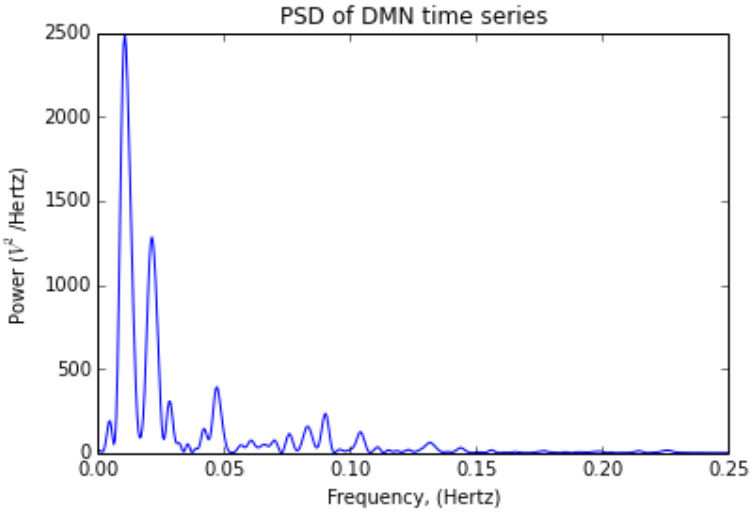

Fig. B.3. Example of a power spectral density of the DMN. It was calculated after detrending with a constant using Welch's method.

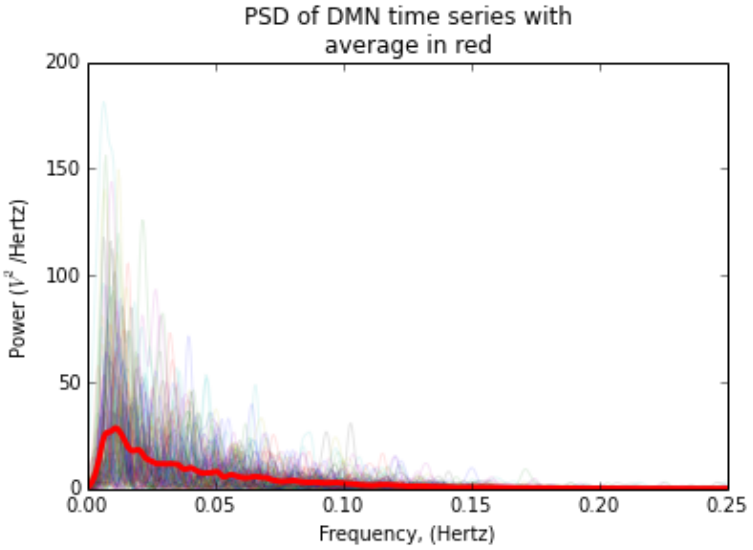

Fig. B.4. Average PSD for the DMN across subjects. There is a large amount of variance.

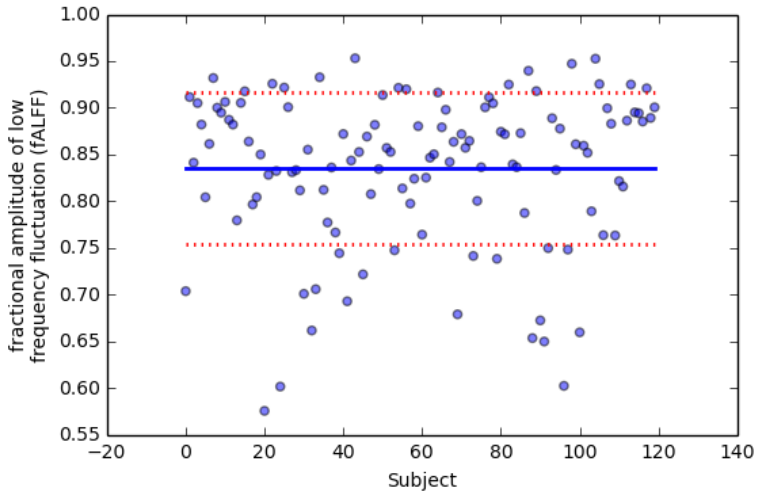

Fig. B.5. Plot of fALFF across subjects.

The metric fALFF was chosen because it did not depend on the scale of the signals, only on the fraction. As an example, Figure B.5 shows some values for multiple subjects. One important note here is that the preprocessing used can dramatically affect these values. As in other areas of fMRI, preprocessing that is suitable for some experiments may not be correct here. For example, most preprocessing involves the use of a high-pass filter, as noise is often considered to have high-frequency components. But performing a high pass filter on this data could invalidate many of the results. As mentioned before, more work is needed to find the right preprocessing and parameters for this type of data.

VITA

VITA

Trey E. Shenk grew up in Indian Cove, Idaho, the son of Mike, a rancher and preacher, and June, a nurse. After completing high school in 2006, Trey attended Pensacola Christian College, earning his Bachelor's Degree *summa cum laude* in 2010. Trey then attended Purdue University, earning his Master's Degree in 2012 before joining the Purdue Neurotrauma Group under advisor Thomas Talavage.